



1 **Tracer-based source apportioning of atmospheric organic carbon and**  
2 **the influence of anthropogenic emissions on secondary organic aerosol**  
3 **formation in Hong Kong**

4 Yubo Cheng<sup>1</sup>, Yiqiu Ma<sup>1,2</sup>, Di Hu<sup>1,2</sup>

5 <sup>1</sup>State Key Laboratory of Environmental and Biological Analysis, Department of Chemistry, Hong Kong Baptist University,  
6 Kowloon Tong, Kowloon, Hong Kong, P. R. China

7 <sup>2</sup>HKBU Institute of Research and Continuing Education, Shenzhen Virtual University Park, Shenzhen, 518057, P. R. China

8 *Correspondence to:* Di Hu ([dihu@hkbu.edu.hk](mailto:dihu@hkbu.edu.hk))



9 **Abstract.** Here we conducted comprehensive chemical characterization and source apportionment of 49 PM<sub>2.5</sub> samples  
10 collected in Hong Kong. Besides the major aerosol constituents, 39 polar organic species, including 14 secondary organic  
11 aerosol (SOA) tracers of isoprene, monoterpenes,  $\beta$ -caryophyllene, and naphthalene, were quantified using gas  
12 chromatography-mass spectrometry (GC-MS). Six factors, i.e., SOA, secondary sulfate (SS), biomass burning (BB)/SOA, sea  
13 salt, marine vessels, and vehicle emissions, were apportioned by positive matrix factorization (PMF) as the major sources of  
14 ambient organic carbon (OC) in Hong Kong. The secondary formation, including OC from SOA, SS, and aging of BB plume,  
15 was the leading contributor to OC (51.4%,  $2.15 \pm 1.37 \mu\text{g C m}^{-3}$ ) throughout the year. We then applied a tracer-based method  
16 (TBM) to estimate the SOA formation from the photo-oxidation of four selected precursors, and monoterpenes SOA was the  
17 most abundant. A Kintecus kinetic model was used to examine the formation channels of isoprene SOA, and the aerosol-phase  
18 ring-opening reaction of isoprene epoxydiols (IEPOX) was found to be the dominant formation pathway. Consistently, IEPOX  
19 tracers contributed 94% of total GC-MS quantified isoprene SOA tracers. The TBM-estimated SOC ( $\text{SOC}_{\text{TBM}}$ ) and PMF-  
20 resolved SOC ( $\text{SOC}_{\text{PMF}}$ ) showed similar temporal trends; however,  $\text{SOC}_{\text{TBM}}$  only accounted for 26.5% of  $\text{SOC}_{\text{PMF}}$ , indicating  
21 a large fraction of ambient SOA was from other reaction pathways/precursors. Results of Pearson's R and multivariate linear  
22 regression analysis showed that NO<sub>x</sub> processing played a key role in both daytime and nighttime SOA production in the region.  
23 SOA formation through nighttime NO<sub>3</sub> oxidation of biogenic VOCs, especially monoterpenes, may have made a considerable  
24 contribution to the SOA loading in Hong Kong. Moreover, sulfate had a significant positive linear relationship with  $\text{SOC}_{\text{PMF}}$   
25 and SS-related SOC, and particle acidity was significantly correlated with SOC from the aging of BB.

## 26 1 Introduction

27 Organic aerosol (OA) is a significant component of ambient fine particulate matter (PM<sub>2.5</sub>). It accounts for 20%-60% of the  
28 total PM<sub>2.5</sub> mass on a global scale (Kanakidou et al., 2005; Van Dingenen et al., 2004; Zhang et al., 2007), and even up to 90%  
29 in rural areas (Kanakidou et al., 2005; Roberts et al., 2001; Zhang et al., 2007). OA is either directly emitted into the atmosphere  
30 from natural (e.g., vegetative detritus, volcano activity) and anthropogenic sources (e.g., biomass burning (BB), vehicle  
31 exhaust, cooking), or secondarily formed through the oxidation of biogenic and anthropogenic gas-phase precursors and the  
32 subsequent partition process or particle-phase reactions (Gelencsér et al., 2007; Hildemann et al., 1996; Hu et al., 2010; Zheng  
33 et al., 2014). Given the varying emission sources, meteorological conditions, and anthropogenic activities worldwide and their  
34 influences on ambient OA composition, aerosol scientists have put many efforts to investigate the atmospheric processes of  
35 OA and their primary and secondary sources, which aid the development of more targeted control policy of PM<sub>2.5</sub> pollution  
36 (Hu et al., 2010; Huang et al., 2014; Schauer et al., 2007; Simoneit, 1999; Stone et al., 2009; Zheng et al., 2005). Huang et al.  
37 (2014) applied positive matrix factorization (PMF) to apportion the sources of OA at four urban locations in China, i.e., Beijing,  
38 Shanghai, Guangzhou, and Xi'an. They found that secondary formation accounted for a predominant fraction of OA (44-71%)



39 at all four sites. Hong Kong, a megacity located on the southern coast of China in the PRD region and a hub port for the South  
40 Asian Pacific region, has its unique OC source characteristics. Hu et al. (2010) incorporated biogenic and anthropogenic SOA  
41 tracers and some POA markers into PMF and resolved seven OA sources in Hong Kong. They found that 45% of OC in Hong  
42 Kong during summertime was from secondary formation, and the number could reach up to 65% on sampling days under  
43 regional pollution from the PRD area.

44 All these studies have illustrated the importance of secondary formation to OA in the ambient atmosphere. However, due  
45 to SOA's complex chemical composition and formation mechanisms, a precise prediction of SOA load from individual  
46 precursors at both regional and global scale is still challenging. An SOA tracer based method (TBM) has been developed to  
47 partially solve this problem, which estimates the amount of SOA and SOC formed from the atmospheric oxidation of selected  
48 VOCs (i.e., isoprene, monoterpenes,  $\beta$ -caryophyllene, toluene, and naphthalene) using the mass ratios of tracer-to-SOA/SOC  
49 obtained from laboratory smog chamber experiments (Kleindienst et al., 2007, 2012). However, TBM can only capture SOC  
50 formation from the above-listed VOC precursors, and it may underestimate the actual SOC levels in the ambient atmosphere  
51 due to the lack of SOA tracer-to-SOC ratio values of a broader range of OA precursors. Therefore, besides the SOA tracer  
52 based method, we have also applied PMF to evaluate the contributions of SOC and primary emissions to OA in the region.

53 Many studies have reported the observational evidence of biogenic SOA enhancement induced by anthropogenic emissions,  
54 such as nitrogen oxides ( $\text{NO}_x$ ) and sulfur dioxide ( $\text{SO}_2$ ) (Huang et al., 2014; Xu et al., 2015; Rattanavaraha et al., 2016).  $\text{NO}_x$   
55 is one of the critical drivers of SOA formation through the photochemical oxidation of VOCs via peroxy radical pathways  
56 (Finlayson-Pitts and Pitts, 2000). Nitrogen dioxide ( $\text{NO}_2$ ) reacts with ozone ( $\text{O}_3$ ) to form  $\text{NO}_3$  radical, a critical nighttime gas  
57 oxidant. Several laboratory studies have reported high SOA yields from the oxidation of biogenic VOCs (BVOCs) by  $\text{NO}_3$   
58 radical (Fry et al., 2009; Ng et al., 2008). Some field studies also revealed that SOA formation from  $\text{NO}_3$  oxidation of BVOCs  
59 occurs during both daytime and nighttime (Brown et al., 2013; Rollins et al., 2013). The effect of  $\text{SO}_2$  on SOA formation was  
60 often explained in the context of particle acidity in laboratory studies, which promotes SOA production through acid-catalyzed  
61 heterogeneous reactions (Jang et al., 2002; Surratt et al., 2010). Sulfate was also suggested to enhance isoprene-SOA formation  
62 by acting as the nucleophiles, providing active aerosol surface area, and through the salting-in effect (Rattanavaraha et al.,  
63 2016; Xu et al., 2015). Recently, Wang et al. (2016) proposed a new sulfate formation pathway in aqueous aerosols through  
64  $\text{NO}_2$  oxidation and ammonium neutralization, and synchronous enhancements of both nitrate and SOA production in aqueous  
65 aerosols were reported. These laboratory and field monitoring studies have shown that the abundance and chemical nature of  
66 ambient OA are significantly influenced by the complex interactions among source emissions, anthropogenic activities,  
67 atmospheric physical/chemical processes, and meteorological conditions (An et al., 2019).

68 In this study, we collected 49  $\text{PM}_{2.5}$  samples at an urban site in Hong Kong during a whole year period. Concentration  
69 levels of 39 polar organic species were quantified using gas chromatography-mass spectrometry (GC-MS), and their



70 temporal/meteorological variations were evaluated. With the input of SOA tracers and primary source markers into PMF, we  
71 quantitatively assessed the contributions of various primary and secondary sources to OC. SOC formed from individual  
72 biogenic (i.e., isoprenes, monoterpenes, and  $\beta$ -caryophyllene) and anthropogenic VOCs (i.e., naphthalene) were estimated  
73 using the TBM. Finally, the impacts of anthropogenic pollutants (e.g.,  $\text{NO}_2$ ,  $\text{O}_3$ ,  $\text{NO}_3$ ,  $\text{SO}_2$ , and tropospheric odd oxygen ( $\text{O}_x$ ))  
74 and  $\text{PM}_{2.5}$  constituents (e.g., sulfate, acidity, and liquid water content) on total and individual SOCs estimated by both TBM  
75 and PMF were evaluated using Pearson's R analysis and multi-linear regression model. This study provides comprehensive  
76 information on the sources of OA and SOA in Hong Kong as well as direct evidence of anthropogenic influences on the SOA  
77 formation in the region, which may serve as the scientific basis for the formulation of the  $\text{PM}_{2.5}$  mitigation policy in the region.

## 78 2 Method

### 79 2.1. Sample collection

80 The  $\text{PM}_{2.5}$  samples were collected on the 12<sup>th</sup> floor of Science Tower in the Campus of Hong Kong Baptist University  
81 ( $114^\circ 15\text{E}$ ,  $22^\circ 13\text{N}$ ,  $\sim 40$  m above the ground), which is a typical urban site.  $\text{PM}_{2.5}$  samples were collected from September 6,  
82 2011, to August 16, 2012, and a total of 49 samples were collected. A high-volume air sampler was used to collect  $\text{PM}_{2.5}$  onto  
83 a quartz fiber filter (20 cm  $\times$  25 cm) at a flow rate of  $1.13 \text{ m}^3 \text{ min}^{-1}$  for 24 h. The quartz fiber filters were prebaked at  $550^\circ\text{C}$   
84 for 24 h to remove organic contaminants. After sampling, the filters were immediately transferred to the laboratory and stored  
85 at  $-18^\circ\text{C}$  until analysis.

### 86 2.2. Chemical analysis

87 For EC and OC analysis, a  $1 \times 1 \text{ cm}^2$  filter was cut and analyzed using a thermal and optical transmittance aerosol carbon  
88 analyzer (Sunset Laboratory, Tigard, OR, USA). Major ions (i.e.,  $\text{Cl}^-$ ,  $\text{NO}_3^-$ ,  $\text{SO}_4^{2-}$ ,  $\text{C}_2\text{O}_4^{2-}$ ,  $\text{Na}^+$ ,  $\text{Ca}^{2+}$ ,  $\text{Mg}^{2+}$ ,  $\text{K}^+$ ,  $\text{NH}_4^+$ ) were  
89 identified and quantified by ion-chromatography (IC, DX500, Dionex, Sunnyvale, CA, USA). Vanadium (V) and Nickel (Ni)  
90 were analyzed using an Agilent 7900 ICP-MS. Detailed analytical methods for the measurements of EC, OC, and ions were  
91 described in our previous work (Hu and Yu, 2013; Ma et al., 2019).

92 Thirty-nine polar organic species were identified and quantified using an Agilent 7890A-5975C GC-MS with prior BSTFA  
93 derivatization (N, O-Bis-(trimethylsilyl)trifluoroacetamide, with 1% trimethylchlorosilane, TMCS). For each aerosol sample,  
94  $20 \text{ cm}^2$  of the filter was cut into small pieces and sonicated for 10 min with 10 mL of distilled acetonitrile (HPLC grade); the  
95 extraction was repeated three times. The extracts were combined and filtered through a Millipore  $0.45\text{-}\mu\text{m}$  PTEE hydrophobic  
96 Teflon filter into a 50 mL round flask, concentrated to  $\sim 0.5$  mL by rotary evaporation, and transferred into a 5 mL reaction  
97 vial. The round flask was rinsed with 1 mL of acetonitrile for three times, and the rinsing solvent was transferred into the  
98 reaction vial as well. The final extract was blown to dryness under a gentle stream of pure nitrogen gas at  $40^\circ\text{C}$  and then



99 derivatized with 100  $\mu\text{L}$  of BSTFA and 50  $\mu\text{L}$  of pyridine at 70  $^{\circ}\text{C}$  for 2 h. After the reaction vial cooled down to room  
100 temperature, 30  $\mu\text{L}$  of tetracosane- $d_{50}$  (internal standard, 50  $\mu\text{g mL}^{-1}$  in hexane) was added. The derivatives were analyzed by  
101 GC-MS. Two microliters of the derivatized sample or standard were injected and separated on an HP-5MS capillary column  
102 (30.0m $\times$ 250 $\mu\text{m}\times$ 0.25 $\mu\text{m}$ , Agilent J&W). The temperature program and instrument settings were adapted from the method used  
103 by Hu et al. (2008).

104 Saccharides, di- and tricarboxylic acids, 4-nitrocatechol, and cholesterol were identified and quantified using authentic  
105 standards. The SOA tracers were identified using surrogate compounds with similar structures and functional groups (Hu et  
106 al., 2008; Hu and Yu, 2013), and the detailed information was provided in Table 1. Recovery tests of these organic species  
107 were carried out by spiking the mixture of standards onto blank quartz filters, followed by the same sample extraction and  
108 analysis processes. Recoveries of the polar compounds were within the range of 80% to 120%. Analysis of hopanes has been  
109 reported in our previous study (Ma et al., 2019). Four hopanes, including 17 $\alpha$ ,21 $\beta$ -hopane, 17 $\alpha$ ,21 $\beta$ -22R-homhopane,  
110 17 $\alpha$ ,21 $\beta$ -22S-homhopane, and 17 $\alpha$ ,21 $\beta$ -30-norhopane, were measured using an Agilent 6890N-5975 GC-MS with thermal  
111 desorption (TD) method. Recoveries of four hopane standards ranged from 83% to 98%.

### 112 3 Results

113 Hourly meteorological and air quality data (i.e., temperature, relative humidity (RH), O<sub>3</sub>, SO<sub>2</sub>, and NO<sub>2</sub>) in the vicinity of  
114 the sampling site were collected by Hong Kong Environmental Protection Department  
115 (HKEPD) (<http://envf.ust.hk/dataview/gts/current/>). During the sampling period, the ambient temperature ranged from 14.52  
116 to 31.01  $^{\circ}\text{C}$ , with an annual average of 24.17 $\pm$ 5.00  $^{\circ}\text{C}$ . The daily average of RH ranged from 52.94% to 97.02%, with a yearly  
117 average of 79.87 $\pm$ 10.54%. Heavy rains are common in Hong Kong during summer, which effectively washes out the PM  
118 pollutants.

119 Hong Kong is located at the south-east edge of the Pearl River Delta (PRD) region. PRD is a rapidly developing area with  
120 intensive industrial activities. Air pollutants origin from the northern PRD region can travel together with air masses and  
121 transport into Hong Kong. Same as in our previous study (Hu et al., 2010; Ma et al., 2019), we carefully examined the air mass  
122 backward trajectories, the spatial distribution patterns of SO<sub>2</sub>, the concentration levels of both PM<sub>2.5</sub> and O<sub>3</sub>, and the synoptic  
123 weather conditions during the sampling period. We then categorized all sampling days into three groups, i.e., days mainly  
124 influenced by the regional pollution from the PRD region (regional days), days influenced by long-regional transport of air  
125 mass from the northern and eastern China (LRT days), and days dominated by the locally generated pollutants (local days).

126 The gas pollutants, i.e., O<sub>3</sub>, NO<sub>2</sub>, O<sub>x</sub>, and SO<sub>2</sub>, showed significantly higher average concentrations on regional days than  
127 those on LRT local days (Table 2). The annual mean concentrations of O<sub>3</sub>, NO<sub>2</sub>, and SO<sub>2</sub> were 14.85 $\pm$ 8.69 ppb, 37.15 $\pm$ 9.76  
128 ppb, and 4.45 $\pm$ 2.57  $\mu\text{g m}^{-3}$ , respectively. Given that O<sub>3</sub> and NO<sub>2</sub> undergo a rapid photochemical conversion in the ambient



129 atmosphere, the tropospheric odd oxygen  $O_x$  (the sum of  $O_3$  and  $NO_2$ ) was calculated as an indicator of atmospheric oxidation  
130 capacity. As shown in Table 1,  $O_x$  ranged from 49.72 to 145.90  $\mu\text{g m}^{-3}$ , with a mean value of  $99.31 \pm 27.42 \mu\text{g m}^{-3}$ , indicating  
131 a high oxidation capacity of the Hong Kong atmosphere. The annual average concentrations of OC and EC were  $4.18 \pm 2.37$   
132 and  $1.02 \pm 0.54 \mu\text{gC m}^{-3}$ , respectively. Ambient OC levels observed on regional days ( $6.15 \pm 2.51 \mu\text{gC m}^{-3}$ ) were about two times  
133 higher than those on LRT and local days; as for EC, it exhibited relative constant levels throughout the year ( $0.14$ - $2.75 \mu\text{gC}$   
134  $\text{m}^{-3}$ ). This confirms that EC is mainly emitted locally in Hong Kong, and OC has some regional sources. Moreover, the OC/EC  
135 ratios of the collected samples ranged from 1.51 to 10.91, with an annual average value of 4.61, indicating secondary formation  
136 could be a dominant source of OA in this region (Mancilla et al., 2015). Our previous study has observed that SOC contributed  
137 45% of OC in Hong Kong during the summer of 2006 (Hu et al., 2008). Here the analysis was expanded to samples taken  
138 during the 1-yr period to obtain a more comprehensive understanding of sources and their contributions to ambient OA in  
139 Hong Kong, and the factors that impact ambient SOA formation.

### 140 3.1 Characterization of SOA tracers and other polar oxygenated organic compounds

141 The concentration levels of 39 organic species, including 14 SOA tracers, 12 saccharides, 11 di- and tricarboxylic acids, 4-  
142 nitrocatechol, and cholesterol, under different meteorological conditions, were listed in Table 1.

#### 143 3.1.1 SOA tracers of isoprene, monoterpenes, $\beta$ -caryophyllene, and naphthalene

144 Seven isoprene SOA ( $Isop_{SOA}$ ) tracers, i.e. 2-methylglyceric acid, two methyltetrol isomers (2-methylthreitol and 2-  
145 methylerythritol), three  $C_5$ -alkene triol isomers (cis-2-methyl-1,3,4-trihydroxy-1-butene, 3-methyl-2,3,4-trihydroxy-1-butene,  
146 and trans-2-methyl-1,3,4-trihydroxy-1-butene), and 3-meTHF-3,4-diols (including both cis- and trans-3-  
147 methyltetrahydrofuran-3,4-diols) were identified and quantified. The sum of all  $Isop_{SOA}$  tracers ranged from 1.67 to 117.17  
148  $\text{ng m}^{-3}$ , with the annual mean value of  $22.78 \pm 26.06 \text{ng m}^{-3}$ . Among the  $Isop_{SOA}$  tracers, methyltetrols and  $C_5$ -alkene triols  
149 were the most abundant, and they are suggested to be formed through the acid-catalyzed ring-opening reactions of IEPOX  
150 under low- $NO_x$  condition (Chan et al., 2010; Surratt et al., 2010). Higher concentrations of  $Isop_{SOA}$  tracers were measured in  
151 summer and autumn than in winter and spring. This could be caused by the higher temperature, stronger solar radiation, and  
152 higher emission of isoprene in summer and autumn than in the other two seasons, which promoted the SOA formation from  
153 isoprene. This seasonal pattern is consistent with what were observed in other studies (Ding et al., 2012; Kleindienst et al.,  
154 2007; Lewandowski et al., 2008). However, if we compare the levels of isoprene tracers monitored at different sites during  
155 summer, the total amount of  $Isop_{SOA}$  tracers measured in Hong Kong was about five times lower than those measured in  
156 several cities in the U.S. and a rural site (WQS site) in the PRD area (Ding et al., 2012; Kleindienst et al., 2007; Lewandowski  
157 et al., 2008). This may be due to the different levels of isoprene, OH radical, and  $NO_x$  at these sampling sites. The 3-MeTHF-



158 3,4-diols, tracers formed through the intermolecular rearrangement of isoprene epoxydiols (IEPOX) under acidic conditions,  
159 was identified in Hong Kong PM<sub>2.5</sub> samples for the first time. It has an annual mean concentration of  $0.23 \pm 0.10$  ng m<sup>-3</sup>, which  
160 was about 70 times lower than that in Birmingham, U.S. (Rattanavara et al., 2016), but was comparable to what was observed  
161 at the WQS site in the PRD area (He et al., 2018). 2-Methylglyceric acid, an isoprene tracer formed from methacrylic acid  
162 epoxide (MAE) and hydroxymethyl-methyl- $\alpha$ -lactone (HMML) under high-NO<sub>x</sub> conditions (Lin et al., 2013; Nguyen et al.,  
163 2015), presented a quite different temporal trend from those of the other six Isop<sub>SOA</sub> tracers, with the highest concentration in  
164 winter, and then autumn, summer, and spring. Chamber studies suggested that MAE is an oxidation product resulting from the  
165 OH addition to methacryloylperoxynitrate (MPAN) and its production is temperature dependant (Roberts and Bertman, 1992;  
166 Worton et al., 2013). Under higher temperatures, the loss of MPAN is dominated by thermal decomposition, which does not  
167 produce SOA tracers through the NO/NO<sub>2</sub> pathway. Under lower temperature, thermal decomposition of MPAN is limited and  
168 more MPAN reacts with OH to generate MAE. Therefore, the lower temperatures in winter would favor the production of  
169 MAE and the MAE Isop<sub>SOA</sub> tracers, such as 2-methylglyceric acid. Moreover, all Isop<sub>SOA</sub> tracers exhibited higher  
170 concentrations on regional days than LRT and local days. On regional days, air masses transported from the PRD area worsened  
171 the air quality in Hong Kong, and the higher levels of gaseous pollutants, e.g., O<sub>3</sub>, NO<sub>2</sub>, O<sub>x</sub>, and SO<sub>2</sub> (Table 2), promoted SOA  
172 formation.

173 Generally speaking, at an urban location with anthropogenic NO<sub>x</sub> emissions from automobiles and power plants, the  
174 generation of Isop<sub>SOA</sub> tracers from the MAE NO/NO<sub>2</sub> pathway should be more favored than the HO<sub>2</sub> IEPOX channel.  
175 However, in this study, 94% of the total mass of the quantified Isop<sub>SOA</sub> tracers were produced through the IEPOX HO<sub>2</sub>  
176 pathway. A similar phenomenon was observed at the WQS site in the PRD region (He et al., 2018). Therefore, to better  
177 understand the influences of environmental factors on isoprene SOA formation in the region, we applied the kinetic models  
178 described by Eddingsaas et al. (2010), Worton et al. (2013), and Birdsall et al. (2014) to investigate the fate of both IEPOX  
179 and MAE in the atmosphere. Besides their degradation through acid-catalyzed ring-opening reactions on particles, IEPOX and  
180 MAE can also be oxidized in the gas phase or removed by dry deposition (Eddingsaas et al., 2010). We applied the Kintecus  
181 kinetic model to quantitatively evaluate the fractions of these two Isop<sub>SOA</sub> intermediates that undergo gas-phase oxidation,  
182 aerosol-phase acid-catalyzed ring-opening reaction, and dry deposition processes. Details of the model calculations were  
183 provided in the appendices.

184 Figure 1 showed the comparison of the three elimination processes of IEPOX and MAE during the sampling period in  
185 Hong Kong. Given the high volatility of MAE (vapor pressure:  $9.2 \times 10^{-5}$  atm) (Worton et al., 2013), it has a low tendency to  
186 partition onto the particle phase and its uptake onto aqueous particles is mainly governed by Henry's law constant ( $k_{H}^{cp}$ ).  
187 Worton et al. (2013) estimated the  $k_{H}^{cp}$  value of MAE to be  $7.5 \times 10^6$  M atm<sup>-1</sup>, which is 20 times lower than that of IEPOX  
188 ( $1.3 \times 10^8$  M atm<sup>-1</sup>). Moreover, Riedel et al. (2015) suggested that the heterogeneous reactive uptake coefficient of MAE ( $\gamma =$



189  $4.9 \times 10^{-4}$ ) through the ring-opening reaction was a factor of 30 lower than that of IEPOX. Therefore, as shown in Figure 1,  
190 MAE was primarily eliminated by dry deposition ( $> 80\%$ ) in the gas phase, and only a trivial fraction was degraded through  
191 the ring-opening reactions ( $\leq 2\%$ ). Our results on the fate of MAE were similar to those observed at the University of  
192 California-Blodgett Forest Research Station (UC-BFRS) (Worton et al., 2013). However, our results on the relative  
193 contributions of these three degradation pathways to IEPOX loss were quite different from theirs, indicating a more sensitive  
194 response of IEPOX than MAE to the change of environmental oxidants and conditions. Given the high liquid water content  
195 (LWC; mean:  $57.20 \pm 37.15 \mu\text{g m}^{-3}$ ) and particle acidity ( $\text{H}_p^+$ ; mean:  $-0.28 \pm 0.42$ ) of  $\text{PM}_{2.5}$  samples in this study (Table 2),  
196 particle-phase ring-opening reaction ( $F_{\text{rop}}$ ) was the dominant degradation pathway of IEPOX in the Hong Kong atmosphere  
197 (average:  $97.6\%$ ), and its loss through dry deposition and gas-phase oxidation is almost negligible. The  $F_{\text{rop}}$  of IEPOX reported  
198 by Worton et al. (2013) was only  $0.02\%$ , mainly due to the much lower LWC (mean:  $0.4 \mu\text{g m}^{-3}$ ) and weaker  $\text{H}_p^+$  (pH mean:  
199  $4.4$ ) of their  $\text{PM}_{2.5}$  samples. These results demonstrated that particle-phase LWC and  $\text{H}_p^+$  played a more significant role in the  
200 atmospheric degradation of IEPOX than MAE. Results from the kinetic model simulation were strongly supported by the  
201 experimental finding of IEPOX tracers as the dominant Isop<sub>SOA</sub> tracers measured in Hong Kong. The average ratio of IEPOX  
202 tracers to MAE tracers was  $16.54$  (ranged from  $3.00$  to  $71.58$ ), and the average value of  $F_{\text{rop-IEPOX}}/F_{\text{rop-MAE}}$  was  $191.92$ ,  
203 confirming that the IEPOX  $\text{HO}_2$  channel is the major formation pathway of isoprene SOA in the region.

204 Five SOA tracers of monoterpenes (Mono<sub>SOA</sub>), i.e., 3-hydroxyglutaric acid, 3-hydroxy-4,4-dimethylglutaric acid, 3-  
205 methyl-1,2,3-butanetricarboxylic acid, 3-isopropylpentanedioic acid, and 3-acetyl pentanedioic acid, were identified and  
206 quantified. Their summed concentrations ranged from  $2.54$  to  $32.57 \text{ ng m}^{-3}$ , with an annual average value of  $10.76 \pm 8.04 \text{ ng m}^{-3}$ ,  
207 comparable to that reported at the WQS site in the PRD region but lower than that measured in the U.S. (Ding et al., 2012;  
208 Kleindienst et al., 2007; Lewandowski et al., 2008). All Mono<sub>SOA</sub> tracers showed the highest level on regional days (mean:  
209  $18.00 \pm 9.28 \text{ ng m}^{-3}$ ), followed by LRT (mean:  $10.31 \pm 7.33 \text{ ng m}^{-3}$ ) and local days (mean:  $6.41 \pm 2.75 \text{ ng m}^{-3}$ ) (Table 1). Although  
210 a higher emission and faster photochemical degradation of monoterpenes are expected in summer due to the intense solar  
211 radiation and high temperature, higher levels of Mono<sub>SOA</sub> tracers were monitored in autumn and winter than in the other two  
212 seasons, similar to what observed at the WQS site (Ding et al., 2014). This seasonal trend of monoterpene SOA tracers may  
213 be partly due to the lower mixing height and temperature during autumn/winter, which favored the partition of Mono<sub>SOA</sub>  
214 tracers onto the aerosol phase. Moreover, most of the regional days were identified in autumn and winter. The higher levels of  
215  $\text{NO}_x$ ,  $\text{O}_3$ ,  $\text{O}_x$ , and  $\text{SO}_2$  on regional days (Table 2) are also responsible for the enhanced monoterpene SOA production in autumn  
216 and winter. Among Mono<sub>SOA</sub> tracers, 3-hydroxyglutaric acid (3HGA) was the most abundant, contributing  $\sim 60\%$  of the total  
217 mass of Mono<sub>SOA</sub> tracers. Smog chamber experiments showed that the production yield of 3-methyl-1,2,3-butanetricarboxylic  
218 acid (MBTCA) from  $\alpha$ -pinene/ $\text{NO}_x$  oxidation was significantly higher than those from the  $\beta$ -pinene/ $\text{NO}_x$  and d-limonene/ $\text{NO}_x$   
219 experiments (Jaoui et al., 2005). Therefore, the ratio of 3HGA/MBTCA was used as a criterion to differentiate SOA from  $\alpha$ -





220 pinene and other monoterpenes (Ding et al., 2014). The value of this ratio was obviously higher on regional days ( $8.58 \pm 2.69$ )  
221 than those on LRT ( $6.64 \pm 3.63$ ) and local days ( $5.62 \pm 3.14$ ), indicating that monoterpenes other than  $\alpha$ -pinene, such as  $\beta$ -pinene  
222 and d-limonene, might have a more significant contribution to SOA on regional days in the region.

223 Beta-caryophyllinic acid is the SOA ( $Cary_{SOA}$ ) tracer of  $\beta$ -caryophyllene, and it ranged from 0.49 to  $5.82 \text{ ng m}^{-3}$ , with  
224 an average annual mean value of  $1.53 \pm 1.07 \text{ ng m}^{-3}$ . Similar to the other SOA tracers,  $\beta$ -caryophyllinic acid showed the highest  
225 concentrations on regional days (mean:  $2.33 \pm 1.21 \text{ ng m}^{-3}$ ) than LRT ( $1.73 \pm 1.16 \text{ ng m}^{-3}$ ) and local days ( $0.94 \pm 0.41 \text{ ng m}^{-3}$ )  
226 (Table 1). For its seasonal trend,  $\beta$ -caryophyllinic acid also exhibited the highest concentration in autumn and winter than the  
227 other two seasons. The SOA tracer of toluene, 2,3-dihydroxy-4-oxopentanoic acid, was undetectable in this study, mainly due  
228 to its trace level in the Hong Kong atmosphere (Hu et al., 2008) and the limited sensitivity of GC-quadrupole MS. Even in our  
229 previous study on a batch of summer  $PM_{2.5}$  samples using a more sensitive GC-ion trap MS, it was barely quantified with a  
230 concentration of less than  $1 \text{ ng m}^{-3}$  in most samples (Hu et al., 2008). Phthalic acid was suggested as the SOA tracer of  
231 naphthalene, given its abundance in both naphthalene-SOA and ambient OA (Kleindienst et al., 2012). With the awareness of  
232 the potential uncertainties, e.g., the primary origin of phthalic acid from biomass burning, we adopted phthalic acid as the SOA  
233 tracer of naphthalene representing the SOA formation from anthropogenic VOCs. The concentration levels of phthalic acid  
234 ranged from 0.80 to  $16.42 \text{ ng m}^{-3}$ , with an average of  $4.31 \pm 3.39 \text{ ng m}^{-3}$ . Similar to the other SOA tracers, it also showed the  
235 highest concentrations on regional days ( $7.16 \pm 3.61 \text{ ng m}^{-3}$ ) than LRT ( $4.97 \pm 3.30 \text{ ng m}^{-3}$ ) and local days ( $2.26 \pm 1.38 \text{ ng m}^{-3}$ )  
236 (Table 1).

### 237 3.1.2 Saccharides and dicarboxylic acids

238 Twelve saccharides, i.e., levoglucosan, arabinol, fructose, meso-erythritol, sucrose, galactosan, mannitol, sorbitol,  
239 galactose, glucose, xylose, and xylitol, have been quantified. Of the 12 saccharides, levoglucosan, the tracer of BB, was by far  
240 the most abundant (range:  $0.64\text{--}474.15 \text{ ng m}^{-3}$ ; mean:  $75.02 \pm 111.43 \text{ ng m}^{-3}$ ). It showed the highest levels on regional days  
241 (about 6 times higher than that on local days), especially during winter when BB activities in the PRD region were most  
242 frequent. Two primary saccharides, i.e., fructose and xylose, also exhibited the highest levels on regional days. They showed  
243 good correlations with levoglucosan ( $R^2 = 0.65$  and  $0.93$ ), suggesting that they could be from BB as well.

244 Among the identified dicarboxylic acids, oxalic acid was the most abundant, followed by terephthalic acid, phthalic acid,  
245 malic acid, succinic acid, and others. Most dicarboxylic acids, including the five most abundant ones, showed higher levels on  
246 regional days; they were found with higher levels in winter and autumn as well. This temporal trend is similar to what we have  
247 observed for  $Mono_{SOA}$  tracers and most saccharides, indicating that regional pollution had a dominant influence on the  
248 abundance of both primary and secondary aerosols in Hong Kong, far exceeding the influence of other environmental  
249 parameters, such as temperature and solar radiation. Atmospheric dicarboxylic acids have various sources. For example, oxalic



250 acid was suggested to be secondarily formed from biogenic emissions and anthropogenic sources (e.g., BB and automobile  
251 exhaust) through both gas-phase reactions and in-cloud processing (Yu et al., 2005). Malic acid was suggested to be the photo-  
252 degradation product of both succinic acid and biogenic SOA compounds (Hu and Yu, 2013). In this study, malic acid was  
253 found to be strongly correlated with 3HGA ( $R^2=0.96$ ) and  $\Sigma\text{Mono}_{\text{SOA}}$  tracers ( $R^2=0.95$ ) throughout the year, providing more  
254 evidence to the hypothesis that malic acid is a late-stage oxidation product of BVOCs, especially monoterpenes (Hu and Yu,  
255 2013). Ambient terephthalic acid was mainly directly emitted from plastic wastes incineration (Simoneit et al., 2005) and was  
256 used as a marker of waste incineration.

257 Besides dicarboxylic acids, two benzenetricarboxylic acids (i.e., 1,2,3- and 1,2,4-benzenetricarboxylic acids), 4-  
258 nitrocatechol, and cholesterol were also quantified. The two benzenetricarboxylic acids were suggested to be the photo-  
259 degradation products of polycyclic aromatic hydrocarbons (PAHs) emitted from the combustion activities (Kautzman et al.,  
260 2010). We have previously identified them in the water-soluble humic-like substances (HULIS) extracts of  $\text{PM}_{2.5}$  samples  
261 collected in Beijing and Hong Kong (Ma et al., 2018, 2019). The annual mean concentrations of 1,2,3- and 1,2,4-  
262 benzenetricarboxylic acids measured in this study were  $2.27\pm 1.97 \text{ ng m}^{-3}$  (range:  $0.47\text{-}9.50 \text{ ng m}^{-3}$ ) and  $3.13\pm 2.68 \text{ ng m}^{-3}$  ( $0.47\text{-}$   
263  $12.54 \text{ ng m}^{-3}$ ), respectively, which were comparable to what measured at the other four sites in the PRD region (He et al., 2018).  
264 The 4-nitrocatechol, which was secondarily generated from the photo-oxidation of naphthalene, was suggested as the tracer of  
265 atmospheric aging of BB plume (Kitanovski et al., 2012). It strongly correlated with levoglucosan ( $R^2=0.88$ ) and exhibited  
266 higher levels on regional days and during winter, which further confirmed its BB origin in the region. Therefore, the two  
267 benzenetricarboxylic acids and 4-nitrocatechol were included in PMF analysis as the SOA tracers of BB aging.

### 268 3.2 Source apportionment of organic aerosols

269 In this study, PMF analysis was performed to determine the major OA sources and quantify their contributions to OC.  
270 Eighteen species were input into PMF, including EC, OC, Ni, V, major ions, and various primary and secondary organic tracers.  
271 Given their similar origins, some organic tracers were lumped together, and the lumped species were used as the fitting species  
272 in PMF. They were (1)  $\text{C}_5$ -alkene triols, sum of the three  $\text{C}_5$ -alkene triols isomers; (2) IsopT, the sum of two methyltetrol  
273 isomers and 2-methyl glyceric acid; (3) MonoT, the sum of the five monoterpenes SOA tracers; and (4) Hopane, the sum of  
274 the four hopanes. Since  $\text{C}_5$ -alkene triols were not in the SOA tracers list of the TBM (Kleindienst et al., 2007), the lumped  $\text{C}_5$ -  
275 alkene triols were used as a separated fitting species in PMF. PMF solutions were tested with 4 to 8 factors. A hundred base  
276 runs were performed in each modeling run, and the run with the minimum Q value was selected. The uncertainty values of  
277 each input species were calculated using the method described in our previous studies (Hu et al., 2010; Ma et al., 2016), which  
278 were set to be 20% of the mean concentrations for OC and EC, and 40% of mean values for cations, anions, and all organic  
279 species. An extra modeling uncertainty of 10% was used to account for possible temporal changes in the source profiles. The



280  $Q_{\text{Robust}}/Q_{\text{True}}$  ratio was 1.00, and scaled residuals were normally distributed between -0.2 and 0.2, indicating no influence of  
281 outliers on the solution. A hundred bootstrap runs were performed with a minimum correlation R-value to examine the base  
282 run solution's stability and uncertainty. All bootstrapped factors were explicitly mapped to factors resolved in base solution  
283 with no exception. In the displacement (DISP) assessment, no error was found, and the drop of Q value was less than 1%,  
284 suggesting a stable solution. No swap factor appeared at  $dQ_{\text{max}}=4$ , indicating there was no considerable rotational ambiguity  
285 in the solution. Rotations were introduced to the solutions by adjusting the FPEAK value from -1 to +1, and the non-rotated  
286 solutions (FPEAK=0.0) were considered to be the most interpretable ones. Moreover, a strong linear correlation between the  
287 measured and PMF-predicted OC ( $OC_{\text{PMF}}$ ) ( $R^2=0.92$ ) was observed, which also suggested a reliable PMF solution. Moreover,  
288 a strong linear correlation between the measured and PMF-predicted OC ( $OC_{\text{PMF}}$ ) ( $R^2=0.92$ ) was observed, which also  
289 suggested a reliable PMF solution.

290 As shown in Figure 2, the first factor was distinguished by high loadings of oxalate and biogenic SOA tracers, suggesting  
291 the secondary origin of this source. The second factor was dominated by large amounts of  $\text{SO}_4^{2-}$  and  $\text{NH}_4^+$ , suggesting the  
292 process of secondary sulfate formation. In the third factor, about 90% of levoglucosan was resolved into it, accompanied by  
293 4-nitrocatechol, phthalic acid, and the two benzenetricarboxylic acids, indicating both the primary emission and aging of BB  
294 plume. Therefore, this factor was defined as BB and SOA (BB/SOA). The fourth factor was identified as vehicular emissions  
295 due to the large amounts of hopanes and EC resolved. The fifth factor has large amounts of Ni and V, which are signatures of  
296 residual oil combustion from the marine vessel (Viana et al., 2009). It is well known that Hong Kong is one of the busiest  
297 container ports globally, which handles 50% of the PRD's total cargo throughput. Therefore, the fifth factor was identified as  
298 marine vessels. The sixth factor has a high loading of  $\text{Na}^+$ ,  $\text{Mg}^{2+}$ , and  $\text{Ca}^{2+}$ , indicating the sea salt source.

299 The two leading sources contributing to ambient OC in Hong Kong were BB (including both primary emission and aging  
300 process,  $OC_{\text{BB}}$ : 27.9%,  $1.17\pm 1.99 \mu\text{gC m}^{-3}$ ) and SOA ( $\text{SOC}_{\text{SOA}}$ : 27.5%,  $1.15\pm 0.82 \mu\text{gC m}^{-3}$ ), followed by marine vessels  
301 ( $OC_{\text{marine}}$ : 15.6%,  $0.65\pm 0.58 \mu\text{gC m}^{-3}$ ), SS ( $\text{SOC}_{\text{SS}}$ : 14.5%,  $0.60\pm 0.46 \mu\text{gC m}^{-3}$ ), vehicle emissions ( $OC_{\text{vehicle}}$ : 10.5%,  $0.44\pm 0.42$   
302  $\mu\text{gC m}^{-3}$ ), and sea salt ( $OC_{\text{sea}}$ : 4.0%,  $0.17\pm 0.19 \mu\text{gC m}^{-3}$ ) (Table 2 and Fig. 3). Since a fraction of SOA from the aging of BB  
303 ( $\text{SOC}_{\text{BB}}$ ) was resolved into the BB/SOA factor, we calculated  $\text{SOC}_{\text{BB}}$  using the following equation:

$$304 \quad \text{SOC}_{\text{BB}} = \text{OC}_{\text{BB}} - \frac{[\text{LEVO}_{\text{BB}}]}{0.082} \quad (1)$$

305 where  $\text{OC}_{\text{BB}}$  and  $[\text{LEVO}_{\text{BB}}]$  are the amounts of OC and levoglucosan resolved in the BB/SOA factor. Using levoglucosan  
306 as the tracer of primarily emitted BB OA, we calculated the amounts of POC from BB ( $\text{POC}_{\text{BB}}$ ) by dividing  $[\text{LEVO}]_{\text{BB}}$  with  
307 0.082, where 0.082 is the average ratio of levoglucosan to POC from the burning of major types of Chinese cereal straws (i.e.,  
308 rice, wheat, and corn) obtained in the combustion chamber experiments (Zhang et al., 2007). As cereal straws are one of the  
309 most common BB fuels in China, the above ratio (0.082) has been used to estimate BB contribution to POC in both Beijing  
310 (Zhang et al., 2008) and Hong Kong (Sang et al., 2011). Therefore, it was adopted to calculate  $\text{POC}_{\text{BB}}$  in this study.



311 Based on PMF results, the source-specific contributions to OC were presented in Table 2 and demonstrated in Fig. 3. The  
312 total SOC apportioned by PMF ( $\text{SOC}_{\text{PMF}}$ ), i.e., the sum of  $\text{SOC}_{\text{SOA}}$ ,  $\text{SOC}_{\text{SS}}$ , and  $\text{SOC}_{\text{BB}}$ , accounted for 51.4% ( $2.15 \pm 1.37 \mu\text{gC}$   
313  $\text{m}^{-3}$ ) of OC in Hong Kong, with the secondary organic-rich sources (i.e.,  $\text{SOC}_{\text{SOA}} + \text{SOC}_{\text{BB}}$ ) contributing 36.9% ( $1.54 \pm 1.13 \mu\text{gC}$   
314  $\text{m}^{-3}$ ) of total OC. Huang et al. (2014) also reported that secondary organic-rich sources accounted for 30–40% of OC in  
315 Guangzhou, another PRD site. A higher level of  $\text{SOC}_{\text{PMF}}$  and its contribution to OC were observed on regional days ( $3.27 \pm 1.18$   
316  $\mu\text{gC m}^{-3}$ , 57.4%) than on LRT ( $2.36 \pm 1.54 \mu\text{gC m}^{-3}$ , 53.0%) and local days ( $1.36 \pm 0.81 \mu\text{gC m}^{-3}$ , 43.6%). An even starker  
317 difference in the amounts of  $\text{SOC}_{\text{BB}}$  between regional and local days was observed, which was eight times higher on the  
318 regional days. This suggested that non-local sources were the dominant contributors to  $\text{SOC}_{\text{BB}}$ . BB activities were intensive in  
319 the PRD region, especially during fall and winter. On regional days, freshly emitted and aged gaseous and aerosol phase  
320 pollutants from the open burning of rice straws and other crops were transported from the northern PRD region into Hong  
321 Kong (Hu et al., 2010). Huang et al. (2014) examined the aging of BB plume at low temperatures. They found that the  
322 production of BB SOA was rapid at a typical OH radical concentration of wintertime China, and the amount of BB SOA may  
323 exceed BB POA in 4–14 h even at  $-10^\circ\text{C}$ . Given that the average temperature in Hong Kong during autumn and winter was  
324  $26.15^\circ\text{C}$  and  $17.76^\circ\text{C}$ , the formation of BB SOA should be even fastly achieved during the regional transport. As expected,  
325  $\text{SOC}_{\text{SOA}}$  also showed a higher average concentration on regional days ( $1.75 \pm 0.75 \mu\text{gC m}^{-3}$ ) than on LRT ( $1.14 \pm 0.82 \mu\text{gC m}^{-3}$ )  
326 and local days ( $0.78 \pm 0.65 \mu\text{gC m}^{-3}$ ), which is consistent with the trends of all SOA tracers. Although SOC from secondary  
327 inorganic-rich source ( $\text{SOC}_{\text{SS}}$ ) exhibited the highest levels ( $0.82 \pm 0.38 \mu\text{gC m}^{-3}$ ) on regional days as well, its contribution to  
328 OC was relatively stable under the three synoptic conditions (Fig. 3). Several studies showed that  $\text{SO}_2$  transported from the  
329 northern PRD region promoted secondary sulfate formation in Hong Kong through both gas-phase and in-cloud oxidation  
330 pathways (Lu and Fung, 2016; Yu et al., 2005; Yuan et al., 2006). A recent study proposed that the sulfate formation in aqueous  
331 aerosols through  $\text{NO}_2$  oxidation and ammonium neutralization can simultaneously enhance the production of both nitrate and  
332 SOA (Wang et al., 2016), which helps explain the considerable amount of  $\text{SOC}_{\text{SS}}$  apportioned.

333 OC from the four primary sources, i.e.,  $\text{POC}_{\text{BB}}$ ,  $\text{OC}_{\text{marine}}$ ,  $\text{OC}_{\text{vehicle}}$ , and  $\text{OC}_{\text{sea}}$ , accounted for 48.6% of total OC throughout  
334 the year. Similar to  $\text{SOC}_{\text{BB}}$ ,  $\text{POC}_{\text{BB}}$  showed a higher level ( $1.38 \pm 1.75 \mu\text{gC m}^{-3}$ ) on regional days due to a large number of  
335 emissions from BB activities in the northern PRD area.  $\text{OC}_{\text{vehicle}}$  remained a higher contribution on local days (15.6%,  
336  $0.49 \pm 0.46 \mu\text{gC m}^{-3}$ ), consistent with our previous finding that vehicle emission is a local pollution source (Hu et al., 2010).  
337 Similarly, marine vessels accounted for a greater amount and larger fraction of OC on local days (32.0%,  $1.00 \pm 0.63 \mu\text{gC m}^{-3}$ )  
338 than LRT (5.2%,  $0.23 \pm 0.19 \mu\text{gC m}^{-3}$ ) and regional days (6.5%,  $0.37 \pm 0.21 \mu\text{gC m}^{-3}$ ). On local days, the southeastern to  
339 southwestern wind brought pollutants from residual oil combustion from the ocean into Hong Kong, leading to a higher  
340  $\text{OC}_{\text{marine}}$ .

341 In summary, both secondary aerosol sources and air mass origins play important roles in atmospheric OC in Hong Kong.



342 On regional days, air mass transported from the northern PRD area brought large amounts of air pollutants into Hong Kong,  
343 which promoted the SOA production from both anthropogenic emissions and BVOCs and resulted in a fraction of 57.4% of  
344 OC being secondarily formed. On the other hand, local sources, including vehicle emissions and marine vessels, became more  
345 critical and significantly contributed to OC (56.4%) on local days.

### 346 3.3 Estimation of SOC origin

347 To better understand the SOA precursors and their contributions to SOA/SOC in the region, we adopted a tracer-based  
348 method (Kleindienst et al., 2007, 2012; Offenberg et al., 2007) to estimate the SOA/SOC formation from a group of selected  
349 biogenic and anthropogenic hydrocarbons, i.e., isoprene, monoterpenes,  $\beta$ -caryophyllene, and naphthalene. The mass ratio of  
350 tracer compounds to the total SOC ( $f_{\text{SOC}}$ ) generated from individual VOC precursors was derived from smog chamber  
351 experiments (Kleindienst et al., 2007; Offenberg et al., 2007). By assuming the same  $f_{\text{SOC}}$  value of the precursor under smog  
352 chamber conditions and in ambient air, one can use the quantified SOA tracer concentrations to estimate the amount of SOC  
353 from that precursor in the real atmosphere. It has been well noted that results obtained from this tracer-based method are subject  
354 to potential uncertainties from various aspects, e.g., the larger variation of precursor concentrations and more complicated  
355 environmental conditions in the real atmosphere than in smog chamber experiments, the decay of some tracer compounds  
356 during transport, mismatch of ambient and smog chamber generated SOA compositions, using surrogates other than ketopinic  
357 acid for the quantification of tracer compounds, and so on (Ding et al., 2014; Hu et al., 2008; Kleindienst et al., 2012, 2007).  
358 However, using the tracer-based method, we can at least have a rough estimation of the key SOA precursors in the region,  
359 their contributions to ambient OC, and the amount of SOC from unknown precursors. Wang et al. (2013) noted that the SOA  
360 tracer-based method would significantly underestimate  $\text{SOC}_{\text{Mono}}$  in the PRD region. Ding et al. (2014) gave a reasonable  
361 explanation that the mismatch of monoterpene tracers measured in ambient air and used to derive  $f_{\text{SOC}}$  of monoterpenes in  
362 chamber studies may increase the uncertainty of  $\text{SOC}_{\text{Mono}}$ . Thus they picked the five  $\text{Mono}_{\text{SOA}}$  tracers measured in their  
363 samples and derived the  $f_{\text{SOC}}$  and  $f_{\text{SOA}}$  values using the SOA tracers data and SOA/SOC concentrations reported by Offenberg  
364 et al. (2007). In this study, we only measured five out of nine monoterpene SOA tracers in Offenberg et al.'s (2007) study.  
365 Similar to Ding et al. (2014), to lower the uncertainty induced from the mismatch of SOA tracer compositions, we derived a  
366  $f_{\text{SOC}_{\text{mono}}}$  value of 0.047 based on Offenberg et al.'s experimental data (2017) and applied it to estimate  $\text{SOC}_{\text{Mono}}$ . Many  
367 research groups have adopted this tracer-based method to assess SOC productions from the five studied VOCs at various  
368 locations in the world, and reasonable results have been obtained (Ding et al., 2012; Fu et al., 2014; Hu et al., 2008; D. Hu and  
369 Yu, 2013; Kleindienst et al., 2012, 2007; Lewandowski et al., 2008).

370 As shown in Table 2, SOC estimated by the tracer-based method ( $\text{SOC}_{\text{TBM}}$ ) ranged from 0.11 to 1.53  $\mu\text{gC m}^{-3}$  in Hong  
371 Kong, accounting for 3.8% to 22.7% of ambient OC levels. It exhibited the same trend as OC and  $\text{SOC}_{\text{PMF}}$ , i.e., with higher



372 concentrations on regional days ( $0.81 \pm 0.35 \mu\text{gC m}^{-3}$ ) than on LRT ( $0.50 \pm 0.29 \mu\text{gC m}^{-3}$ ) and local days ( $0.28 \pm 0.13 \mu\text{gC m}^{-3}$ ).  
373 Similar to our previous study, monoterpenes were found to be the most significant SOC contributor in the region, with  
374  $\text{SOC}_{\text{Mono}}$  ranging from 0.05 to  $0.69 \mu\text{gC m}^{-3}$  and having an average concentration of  $0.23 \pm 0.17 \mu\text{gC m}^{-3}$ .  $\text{SOC}_{\text{Iso}}$  and  $\text{SOC}_{\text{Cary}}$ ,  
375 on the other hand, were about three times smaller than  $\text{SOC}_{\text{Mono}}$  and were  $0.08 \pm 0.09 \mu\text{gC m}^{-3}$  and  $0.07 \pm 0.05 \mu\text{gC m}^{-3}$ ,  
376 respectively. Smog chamber experiments have been carried out to study the SOA yields from  $\cdot\text{OH}$  oxidation, ozonolysis, and  
377 nitrate radical ( $\text{NO}_3$ ) oxidation of monoterpenes and isoprene, and monoterpenes were found to be more effective in SOA  
378 production than isoprene (Lee et al., 2006a, 2006b). Highly oxygenated organic molecules with low and extremely low  
379 volatility were formed from the oxidation of monoterpenes and observed in both laboratory experiments and field  
380 measurements (Ehn et al., 2014; Jokinen et al., 2015; Zhang et al., 2018). Moreover, a synergistic  $\text{O}_3 + \text{OH}$  oxidation pathway  
381 of monoterpenes was recently proposed, which leads to the formation of extremely low-volatility oligomers and may result in  
382 even larger monoterpene SOA yields in the real atmosphere than what observed in the smog chamber experiments (Kenseth et  
383 al., 2018). Tsui et al. (2009) reported a total BVOC emission of  $8.6 \times 10^9 \text{ gC yr}^{-1}$  in Hong Kong, with 40% from monoterpenes  
384 and 30% from isoprene. The remaining 30% could be sesquiterpenes (e.g.,  $\beta$ -caryophyllene) or other BVOCs. Therefore, the  
385 predominance of monoterpenes SOA in BVOCs-derived SOC is likely due to the combined effects of their high SOA yields  
386 and large emissions in the region. Like the SOA tracers, SOC from the four precursors all showed the highest level on regional  
387 days than those on LRT and local days (Table 2). On regional days, large amounts of VOC precursors and gaseous oxidants  
388 could be brought into Hong Kong through the regional transport of air masses from northern PRD and oxidized along the way.  
389 Conversely, on local days, the ocean breeze brings clean air masses from the South China Sea into Hong Kong, leading to a  
390 dilution effect of local air pollution. These results highlight that mass origins play an important role in the SOC formation from  
391 both biogenic and anthropogenic VOCs. Given that  $\text{SOC}_{\text{TBM}}$  is calculated based on the concentration levels of individual SOA  
392 tracers measured in the ambient aerosols, it is reasonable that SOC attributed to each VOC precursor showed the same  
393 meteorological variations as their SOA tracers.

394 We observed similar temporal trends between  $\text{SOC}_{\text{PMF}}$  and  $\text{SOC}_{\text{TBM}}$  ( $R^2=0.71$ ). However,  $\text{SOC}_{\text{TBM}}$  only accounted for  
395 26.5% of  $\text{SOC}_{\text{PMF}}$ , suggesting SOC must have been underestimated by the tracer-based method. A reasonable explanation is  
396 that secondary formation from nighttime reactions, multi-phase reactions, and other SOA precursors are not considered in the  
397 SOA tracer-based method. Because parameters used in the tracer-based method were derived from pure gas-phase photo-  
398 oxidation of VOC precursors in smog chambers (Kleindienst et al., 2007, 2009). Therefore, it is better to be used as a  
399 complementary method with PMF in the source apportionment study of ambient OC, especially SOC.

#### 400 3.4 Effects of anthropogenic influences on secondary aerosol formation

401 Increasing evidence from laboratory studies and ambient observations has shown that anthropogenic emissions can



402 significantly affect SOA formation from terpenoids through multiple chemical processes in both daytime and nighttime (Xu et  
403 al., 2013; Zhang et al., 2018). We conducted the Pearson's R correlation analysis of all SOC terms (i.e., SOC<sub>Iso</sub>, SOC<sub>Mono</sub>,  
404 SOC<sub>Cary</sub>, SOC<sub>Nap</sub>, SOC<sub>TBM</sub>, SOC<sub>PMF</sub>, SOC<sub>BB</sub>, SOC<sub>SOA</sub>, and SOC<sub>SS</sub>) with O<sub>3</sub>, NO<sub>2</sub>, SO<sub>2</sub>, O<sub>X</sub>, NO<sub>3</sub>, sulfate, particle acidity (H<sub>p</sub><sup>+</sup>),  
405 and particle liquid water content (LWC<sub>p</sub>) (Table 3). Details on the calculation of H<sub>p</sub><sup>+</sup> and LWC<sub>p</sub> were presented in Appendix  
406 B. Since NO<sub>3</sub> was not directly monitored at HKEPD stations, its mixing ratio was estimated using the following equation:

$$407 \quad [NO_3] = \frac{k_1[O_3][NO_2]}{\sum k_i[VOC_i]} \quad (2)$$

408 The numerator is the production of NO<sub>3</sub> (p[NO<sub>3</sub>]) from O<sub>3</sub> and NO<sub>2</sub>, and the denominator is the reactivity of NO<sub>3</sub> for NO<sub>3</sub>-  
409 VOCs reactions. From the IUPAC database, we obtained the temperature-dependent expression of *k<sub>l</sub>* (cm<sup>3</sup> molecules<sup>-1</sup> s<sup>-1</sup>), the  
410 production rate constant of NO<sub>3</sub> as 1.4E-13EXP(-2470/T), where T is the ambient temperature in Kelvin. Therefore, using *k<sub>l</sub>*  
411 and the measured concentration levels of [O<sub>3</sub>] and [NO<sub>2</sub>], we calculated p[NO<sub>3</sub>] (Table 2). Brown et al. (2016) reported a NO<sub>3</sub>-  
412 VOCs reactivity of 6.5±6.8×10<sup>-3</sup> s<sup>-1</sup> in Hong Kong with a corresponding NO<sub>3</sub> lifetime of 2.5 min. NO<sub>3</sub> was then calculated as  
413 the ratio of p[NO<sub>3</sub>] to this NO<sub>3</sub> reactivity value, and an annual mean level of 70±47 ppt was estimated.

414 As we mentioned earlier, O<sub>X</sub> is an indicator of atmospheric oxidation capacity. Five SOC terms, i.e., SOC<sub>Mono</sub>, SOC<sub>Nap</sub>,  
415 SOC<sub>TBM</sub>, SOC<sub>SOA</sub>, and SOC<sub>PMF</sub>, showed significant positive correlations with O<sub>X</sub>, especially SOC<sub>SOA</sub> and SOC<sub>PMF</sub> (R>0.7,  
416 P<0.01). However, only SOC<sub>SOA</sub> and SOC<sub>SS</sub> were found to be significantly correlated with O<sub>3</sub> (R>0.50, P<0.01). As for NO<sub>2</sub>,  
417 another critical component of O<sub>X</sub>, it exhibited statistically significant positive correlations with not only SOC<sub>SOA</sub> and SOC<sub>PMF</sub>,  
418 but also several TBM estimated SOCs, including SOC<sub>TBM</sub>, SOC<sub>Mono</sub>, SOC<sub>Nap</sub>, and SOC<sub>Cary</sub>. This may be because SOA tracers  
419 used in TBM were produced from the photo-oxidation of these VOC precursors in the presence of NO<sub>X</sub> (Kleindienst et al.,  
420 2007). The significant positive correlations between NO<sub>2</sub> and SOC<sub>SOA</sub> and SOC<sub>PMF</sub> also suggests that the daytime oxidation  
421 processes involving NO<sub>X</sub> are critical SOA formation pathways in the region. Significant correlations with R>0.5 between NO<sub>3</sub>  
422 and SOC<sub>Mono</sub>, SOC<sub>SOA</sub>, SOC<sub>PMF</sub>, and SOC<sub>SS</sub> were also observed. BVOCs were found to account for >80% of the NO<sub>3</sub> reactivity  
423 in Hong Kong (Brown et al., 2016), with monoterpenes as the leading contributor. Both Zhang et al. (2018) and Xu et al. (2013)  
424 have reported an enhancement of nighttime monoterpenes SOA in the southeastern U.S. by NO<sub>3</sub>-monoterpenes reactions.  
425 Therefore, our findings indicate that SOA formation through nighttime NO<sub>3</sub> oxidation of biogenic VOCs, especially  
426 monoterpenes, may have made a considerable contribution to the SOA loading in Hong Kong. Since NO<sub>3</sub> is a key precursor  
427 of nighttime production of HNO<sub>3</sub>, and nitrate is a significant component of secondary inorganic aerosols, it rationalized the  
428 correlations between NO<sub>3</sub> and SOC<sub>SS</sub>. Six SOC terms, i.e., SOC<sub>Mono</sub>, SOC<sub>Nap</sub>, SOC<sub>TBM</sub>, SOC<sub>SOA</sub>, SOC<sub>SS</sub>, and SOC<sub>PMF</sub>, showed  
429 significant positive correlations with sulfate, especially SOC<sub>SS</sub> and SOC<sub>PMF</sub> (R≥0.8, P<0.01). Given that sulfate is the key  
430 component of secondary inorganic aerosol, such a strong correlation between SOC<sub>SS</sub> and sulfate is expected. Moreover, several  
431 studies have suggested that sulfate also plays a dominant role in the production of aerosol-phase organosulfates through both  
432 nucleophilic addition reactions and the salting-in effect (Lin et al., 2012; Riva et al., 2015; Xu et al., 2015).



433 We then performed multivariate linear regression (MLR) analysis to obtain a quantitative and comprehensive understanding  
434 of the impacts of gaseous oxidants and aerosol characteristics on  $\text{SOC}_{\text{TBM}}$ ,  $\text{SOC}_{\text{PMF}}$ , and the individual PMF resolved SOC  
435 (i.e.,  $\text{SOC}_{\text{SS}}$ ,  $\text{SOC}_{\text{SOA}}$ , and  $\text{SOC}_{\text{BB}}$ ). Six parameters, namely  $\text{O}_3$ ,  $\text{NO}_2$ ,  $\text{NO}_3$ , sulfate,  $\text{H}_p^+$ , and  $\text{LWC}_p$ , were included in the  
436 preliminary runs. However, the MLR results showed that  $\text{O}_3$  was an insignificant factor for all SOC terms, even with negative  
437 regression coefficients. Pearson's R analysis also showed that SOC was more  $\text{NO}_2$  dependent than  $\text{O}_3$ . Therefore, it was  
438 excluded from the final MLR analysis, and the results were shown in Table 4.

439 We found that three parameters, i.e.,  $\text{NO}_2$ , sulfate, and  $\text{NO}_3$ , have statistically significant positive linear relationships ( $P \leq$   
440 0.001) with  $\text{SOC}_{\text{SS}}$ , and the regression coefficients were 0.303, 0.913, and 0.234, respectively. The result is reasonable and  
441 consistent with what was observed from the Pearson's R analysis, given that sulfate is the critical component in the PMF  
442 resolved SS factor, and both  $\text{NO}_2$  and  $\text{NO}_3$  are the precursors of nitrate through  $\text{HNO}_3$  formation. As for  $\text{SOC}_{\text{BB}}$ , three  
443 parameters, i.e.,  $\text{NO}_2$ ,  $\text{NO}_3$ , and  $\text{H}_p^+$ , showed significant positive linear relationships with it ( $P < 0.01$ ), with a regression  
444 coefficient of 0.639, 0.509, and 0.503, respectively. This indicates that  $1 \text{ mol L}^{-1}$  increase in particle acidity was associated  
445 with a  $0.503 \mu\text{gC m}^{-3}$  increase in SOC from BB aging. Phenols, which are produced from the combustion of lignin, are a typical  
446 class of gaseous compounds emitted in large amounts from BB (Bruns et al., 2016; Schauer et al., 2001). Recent laboratory  
447 studies indicate that phenols can undergo multiphase photochemical reactions in the atmosphere with the formation of  
448 nitrophenols and nitrocatechols (Finewax et al., 2018; Yu et al., 2014). Vione et al. (2001) observed the aqueous phase  
449 photonitration of phenols, which was pH-dependent with more nitro-compounds generated at lower pH. Given the strong  
450 particle acidity (pH annual mean: -0.28) observed in the Hong Kong atmosphere, the formation of the 4-nitrocatechol and its  
451 analogs may be favored in the BB plume, which enhances  $\text{SOC}_{\text{BB}}$  formation.

452 Both sulfate and  $\text{NO}_2$  were found as the statistically significant factors that positively correlated with  $\text{SOC}_{\text{PMF}}$ , with  
453 regression coefficients of 0.53 and 0.37, respectively ( $P < 0.001$ , Table 4). This suggests reducing the sulfate level by  $1 \mu\text{g m}^{-3}$   
454 and  $\text{NO}_2$  level by 1 ppb could lower the total PMF-apportioned SOC by 0.53 and  $0.37 \mu\text{gC m}^{-3}$ , respectively.  $\text{NO}_2$  was also  
455 the most significant factor influencing  $\text{SOC}_{\text{TBM}}$ , with a regression coefficient of 0.38 ( $P < 0.001$ ), indicating that a decrease of  
456  $\text{NO}_2$  by 1 ppb can reduce  $\text{SOC}_{\text{TBM}}$  by  $0.38 \mu\text{gC m}^{-3}$ . As for  $\text{SOC}_{\text{SOA}}$ , we found  $\text{NO}_3$  as the most significant parameter ( $P < 0.01$ ),  
457 and a decrease of 1 ppb  $\text{NO}_3$  can lead to a reduction of  $\text{SOC}_{\text{SOA}}$  by  $0.38 \mu\text{gC m}^{-3}$  when holding other covariates unchanged.  
458 These results are consistent with what was observed from the Pearson's R analysis, indicating the importance of NOx  
459 processing on both daytime and nighttime SOA production in the region.

#### 460 4 Conclusions

461 In this study, we identified and quantitatively assessed the contributions of six primary and secondary sources to ambient  
462 OC in Hong Kong, and secondary formation was found to be the leading contributor. Anthropogenic emissions, including  $\text{NO}_2$ ,





463 O<sub>x</sub>, NO<sub>3</sub>, and sulfate, significantly influenced SOA formation in the region. In particular, NO<sub>x</sub> processing in both daytime and  
464 nighttime has played a critical role. Although the ambient NO<sub>2</sub> level has dropped by 33.3% from 1999 to 2019 (the government  
465 of HKSAR, <https://www.info.gov.hk/gia/general/202001/20/P2020012000874.htm>) and sulfate level in PM<sub>2.5</sub> was also  
466 lowered by about 30% from 2000 to 2016 (HKEPD, 2017), the roadside NO<sub>2</sub> level was still high. According to the 20-year air  
467 pollutants monitoring data released by HKSAR, the annual average concentration of roadside NO<sub>2</sub> was much higher than the  
468 other gaseous pollutants, and it peaked during 2011-2013, which were 122 and 118 μg m<sup>-3</sup> in 2011 and 2012, respectively.  
469 Although the annual ambient level of roadside NO<sub>2</sub> decreased to 80 μg m<sup>-3</sup> in 2019, it is still two times higher than the annual  
470 objective level set by the HKSAR government, indicating a continuous significant impact of NO<sub>x</sub> on SOA formation in Hong  
471 Kong, especially in areas with heavy traffic load. Given that 90% of the roadside NO<sub>2</sub> was from commercial vehicles, such as  
472 buses, trucks, minibuses, and so on, our results suggest that more stringent control of NO<sub>x</sub> emission from commercial vehicles  
473 is needed. This will benefit the community by reducing not only the background NO<sub>x</sub> levels but also the SOA pollution in  
474 Hong Kong.

## 475 Appendices

### 476 Appendix A: Kinetic model of loss of isoprene intermediates

477 In this study, we use Kintecus, a kinetics simulation software, to investigate the degradation pathways of two isoprene SOA  
478 intermediates, i.e., IEPOX and MAE, in the atmosphere. Simulation time was set to be 100 h to ensure the completion of  
479 reactions. As described by Eddingsass et al. (2010) and Worton et al. (2013), IEPOX and MAE are removed from the  
480 atmosphere mainly through three pathways, namely the gas-phase photo-oxidation, dry deposition, and aerosol phase acid-  
481 catalyzed ring-opening reaction. Reaction constants that are involved in these three degradation processes were listed below.

IEPOX:

$$k_{\text{OX}} = 5.78 \times 10^{-11} \cdot e^{-400/T} \cdot [\text{OH}] \text{ s}^{-1}$$

$$k_{\text{dd}} = dv/\text{blh} \text{ s}^{-1}$$

$$k_{\text{H}^+} = 5 \times 10^{-2} \cdot [\text{H}_3\text{O}^+] \text{ s}^{-1}$$

$$k_{\text{H}}^{\text{cp}} = 1.3 \times 10^8 \text{ M atm}^{-1}$$

MAE:

$$k'_{\text{OX}} = 1.0 \times 10^{-12} \cdot [\text{OH}] \text{ s}^{-1}$$

$$k'_{\text{dd}} = dv/\text{blh} \text{ s}^{-1}$$

$$k'_{\text{H}^+} = 5.91 \times 10^{-5} \cdot [\text{H}_3\text{O}^+] \text{ s}^{-1}$$

$$k'_{\text{H}}^{\text{cp}} = 7.5 \times 10^6 \text{ M atm}^{-1}$$

482 The eight terms, i.e.,  $k_{\text{OX}}$  and  $k'_{\text{OX}}$ ,  $k_{\text{dd}}$  and  $k'_{\text{dd}}$ ,  $k_{\text{H}^+}$  and  $k'_{\text{H}^+}$ , and  $K_{\text{H}}^{\text{cp}}$  and  $K'_{\text{H}}^{\text{cp}}$ , are the gas-phase oxidation rate  
483 constants, dry deposition rate constants, acid-catalyzed ring-opening rate constants, and Henry's law constants of IEPOX and  
484 MAE, respectively. Given the annual average OH radical level in the PRD region was  $5 \times 10^6$  molecules cm<sup>-3</sup> (Hofzumahaus et  
485 al., 2009),  $k_{\text{OX}}$  and  $k'_{\text{OX}}$  were calculated to be  $7.55 \times 10^{-5} \text{ s}^{-1}$  and  $5.12 \times 10^{-6} \text{ s}^{-1}$  at 298 K.  $k_{\text{dd}}$  is estimated by the deposition  
486 velocity ( $dv$ ) and the boundary layer height ( $\text{blh}$ ). Like Eddingsass et al. (2010) and Worton et al. (2013), we assumed the same



487 deposition velocities for IEPOX and MAE as that for hydrogen peroxide ( $1\text{--}5\text{ cm s}^{-1}$ ). With the predicted boundary height in  
488 Hong Kong of 1100 m (Xie et al., 2012),  $k_{\text{dd}}$  and  $k'_{\text{dd}}$  were calculated to be  $5.05 \times 10^{-5}\text{ s}^{-1}$ . Given the high volatility of MAE  
489 vapor pressure ( $9.2 \times 10^{-5}\text{ atm}$ ) (Worton et al., 2013), it has a low tendency to partition onto the particle phase and its uptake  
490 onto aqueous particles is mainly governed by Henry's law constant ( $k_{\text{H}}^{\text{cp}}$ ). Worton et al. (2013) estimated the  $k_{\text{H}}^{\text{cp}}$  value of  
491 MAE to be  $7.5 \times 10^6\text{ M atm}^{-1}$ , which is 20 times lower than that of IEPOX ( $1.3 \times 10^8\text{ M atm}^{-1}$ , Minerath et al., 2008). Moreover,  
492 Riedel et al. (2015) suggested that the heterogeneous reactive uptake coefficient of MAE ( $\gamma = 4.9 \times 10^{-4}$ ) through the ring-  
493 opening reaction was a factor of 30 lower than that of IEPOX. The ring-opening rate constant ( $k_{\text{H}^+}$ ) for IEPOX and MAE were  
494 estimated by Eddingsaas et al. (2010) and Birdsall et al. (2014), which are  $5 \times 10^{-2}\text{ M}^{-1}\text{ s}^{-1}$  and  $5.91 \times 10^{-5}\text{ M}^{-1}\text{ s}^{-1}$ , respectively.  
495 We then inputted all these parameters into the Kintecus model and estimated the fractions of IEPOX and MAE degraded  
496 through the above mentioned three pathways.

#### 497 **Appendix B: Calculation of particle acidity and total liquid water content**

498 A thermodynamic *model (E-AIM model II)* was applied to estimate the hydrogen ion concentration in air ( $\text{H}^+_{\text{air}}$ ) and liquid  
499 water content associated with inorganic species ( $\text{LWC}_{\text{inorg}}$ ). The liquid water content associated with organic species ( $\text{LWC}_{\text{org}}$ )  
500 was calculated using the following equation

$$501 \quad \text{LWC}_{\text{org}} = \frac{m_{\text{org}} \rho_w}{\rho_{\text{org}}} \frac{k_{\text{org}}}{(1/\text{RH} - 1)}$$

502 where  $k_{\text{org}}$  is an organic hygroscopicity parameter and has a value of 0.1,  $m_{\text{org}}$  is organic mass concentration, and a factor  
503 of 2.1 was applied to convert OC to OM at the urban location.  $\rho_w$  is the water density, and a typical value of  $1.4\text{ g cm}^{-3}$  was  
504 applied for organic aerosols ( $\rho_{\text{org}}$ ). Since LWC is associated with both inorganic and organic species, the total particle water  
505 ( $\text{LWC}_p$ ) was calculated as the sum of  $\text{LWC}_{\text{inorg}}$  and  $\text{LWC}_{\text{org}}$  based on the assumption that particles were internally well mixed.

506 Particle acidity was calculated using the following equation:

$$507 \quad \text{H}^+_p = \frac{1000 \text{H}^+_{\text{air}}}{\text{LWC}_{\text{org}} + \text{LWC}_{\text{inorg}}}$$

508 where  $\text{H}^+_p$  ( $\text{mol L}^{-1}$ ) is the concentration of hydrogen ion in aerosol water, interpreted as particle acidity.  $\text{H}^+_{\text{air}}$  and  $\text{LWC}_{\text{inorg}}$   
509 were calculated by E-AIM model II using input values of inorganic ions, RH, and temperature.

510 **Data availability.** Raw data used in this study are archived at Hong Kong Baptist University, and are available upon request  
511 by contacting the corresponding author.

512 **Author contributions.** YBC and DH designed the study. YBC did all the experiments and most of the data analysis. YQM  
513 helped model analysis and data interpretation. YBC drafted the manuscript. DH helped with data analysis and interpretation  
514 and revised the manuscript.

515 **Competing interest.** The authors declare that they have no conflict of interest.



516

517 **Acknowledgment**

518 This work was supported by the National Natural Science Foundation of China (21976151 and 21477102) and the General  
519 Research Fund of Hong Kong Research Grant Council (12328216, 12304215, 12300914). The authors thank the  
520 Environmental Central Facility (ENVF) in Hong Kong University of Science and Technology (HKUST) for real-time  
521 environmental and air quality data (<http://envf.ust.hk/dataview/gts/current/>).



## 522 References

- 523 An, Z., Huang, R.J., Zhang, R., Tie, X., Li, G., Cao, J., Zhou, W., Shi, Z., Han, Y., Gu, Z., Ji, Y.: Severe haze in northern China:  
524 A synergy of anthropogenic emissions and atmospheric processes, *Proc. Natl. Acad. Sci. U. S. A.*, 116, 8657–8666,  
525 <https://doi.org/10.1073/pnas.1900125116>, 2019.
- 526 Barbara J. Finlayson-Pitts, James N. Pitts, J.: *Chemistry of the upper and lower atmosphere*, Academic Press,  
527 <https://doi.org/https://doi.org/10.1016/B978-0-12-257060-5.X5000-X>, 2000.
- 528 Birdsall, A.W., Miner, C.R., Mael, L.E., Elrod, M.J.: Mechanistic study of secondary organic aerosol components formed from  
529 nucleophilic addition reactions of methacrylic acid epoxide, *Atmos. Chem. Phys.*, 14, 12951–12964,  
530 <https://doi.org/10.5194/acp-14-12951-2014>, 2014.
- 531 Brown, S.S., Dubé, W.P., Bahreini, R., Middlebrook, A.M., Brock, C.A., Warneke, C., De Gouw, J.A., Washenfelder, R.A.,  
532 Atlas, E., Peischl, J., Ryerson, T.B., Holloway, J.S., Schwarz, J.P., Spackman, R., Trainer, M., Parrish, D.D., Fehsenfeld,  
533 F.C., Ravishankara, A.R.: Biogenic VOC oxidation and organic aerosol formation in an urban nocturnal boundary layer:  
534 Aircraft vertical profiles in Houston, TX, *Atmos. Chem. Phys.*, 13, 11317–11337. [https://doi.org/10.5194/acp-13-11317-](https://doi.org/10.5194/acp-13-11317-2013)  
535 2013, 2013.
- 536 Brown, S.S., Dubé, W.P., Tham, Y.J., Zha, Q.Z., Xue, L.K., Poon, S., Wang, Z., Blake, D.R., Tsui, W., Parrish, D.D., Wang, T.:  
537 Nighttime chemistry at a high altitude site above Hong Kong, *J. Geophys. Res. Atmos.*, 121, 2457–2475, doi:10.1002/  
538 2015JD024566, 2016.
- 539 Bruns, E.A., El Haddad, I., Slowik, J.G., Kilic, D., Klein, F., Baltensperger, U., Prévôt, A.S.H.: Identification of significant  
540 precursor gases of secondary organic aerosols from residential wood combustion, *Sci. Rep.*, 6, 27881.  
541 <https://doi.org/10.1038/srep27881>, 2016.
- 542 Chan, M.N., Surratt, J.D., Claeys, M., Edgerton, E.S., Tanner, R.L., Shaw, S.L., Zheng, M., Knipping, E.M., Eddingsaas, N.C.,  
543 Wennberg, P.O., Seinfeld, J.H.: Characterization and quantification of isoprene-derived epoxydiols in ambient aerosol  
544 in the southeastern united states, *Environ. Sci. Technol.*, 44, 4590–459, <https://doi.org/10.1021/es100596b>, 2010.
- 545 Ding, X., Wang, X.M., Gao, B., Fu, X.X., He, Q.F., Zhao, X.Y., Yu, J.Z., Zheng, M.: Tracer-based estimation of secondary  
546 organic carbon in the Pearl River Delta, South China, *J. Geophys. Res. Atmos.*, 117, D05313,  
547 <https://doi.org/10.1029/2011JD016596>, 2012.
- 548 Ding, X., He, Q., Shen, R., Yu, Q., Wang, X., Guenther, D., Dlugokencky, E., Lang, P., Newberger, T., Wolter, S., White, A.,  
549 Noone, D., Wolfe, D., Schnell, R., Ding, X., He, Q., Shen, R., Yu, Q., Wang, X.: Spatial distributions of secondary  
550 organic aerosols from isoprene, monoterpenes,  $\beta$ -caryophyllene, and aromatics over China during summer, *J. Geophys.*  
551 *Res. Atmos.*, 119, 11877–11891, <https://doi.org/10.1002/2014JD02174>, 2014.
- 552 Eddingsaas, N.C., Vandernelde, D.G., Wennberg, P.O.: Kinetics and products of the acid-catalyzed ring-opening of  
553 atmospherically relevant butyl epoxy alcohols, *J. Phys. Chem. A*, 114, 8106–8113, <https://doi.org/10.1021/jp103907c>,  
554 2010.
- 555 Ehn, M., Thornton, J.A., Kleist, E., Sipilä, M., Junninen, H., Pullinen, I., Springer, M., Rubach, F., Tillmann, R., Lee, B.,  
556 Lopez-Hilfiker, F., Andres, S., Acir, I.H., Rissanen, M., Jokinen, T., Schobesberger, S., Kangasluoma, J., Kontkanen, J.,  
557 Nieminen, T., Kurtén, T., Nielsen, L.B., Jørgensen, S., Kjaergaard, H.G., Canagaratna, M., Maso, M.D., Berndt, T., Petäjä,  
558 T., Wahner, A., Kerminen, V.M., Kulmala, M., Worsnop, D.R., Wildt, J., Mentel, T.F.: A large source of low-volatility  
559 secondary organic aerosol, *Nature*, 506, 476–479, <https://doi.org/10.1038/nature13032>, 2014.
- 560 Environmental Protection Department of Hong Kong, Hong Kong emission inventory report.  
561 [https://www.epd.gov.hk/epd/sc\\_chi/environmentinhk/air/data/emission\\_inve.html](https://www.epd.gov.hk/epd/sc_chi/environmentinhk/air/data/emission_inve.html), 2017.
- 562 Finewax, Z., De Gouw, J.A., Ziemann, P.J.: Identification and quantification of 4-nitrocatechol formed from OH and NO<sub>3</sub>  
563 radical-initiated reactions of catechol in air in the presence of NOx: Implications for secondary organic aerosol formation  
564 from biomass burning, *Environ. Sci. Technol.*, 52, 1981–1989, <https://doi.org/10.1021/acs.est.7b05864>, 2018.



- 565 Fry, J.L., Rollins, a W., Wooldridge, P.J., Brown, S.S., Fuchs, H., Dub, W.: Organic nitrate and secondary organic aerosol  
566 yield from NO<sub>3</sub> oxidation of β-pinene evaluated using a gas-phase kinetics/aerosol partitioning model, *Atmos. Chem.*  
567 *Phys.*, 9, 1431–1449, <https://doi.org/10.5194/acp-9-1431-2009>, 2009.
- 568 Fu, P., Kawamura, K., Chen, J., Miyazaki, Y.: Secondary production of organic aerosols from biogenic VOCs over Mt. Fuji,  
569 Japan, *Environ. Sci. Technol.*, 48, 8491–8497, <https://doi.org/10.1021/es500794d>, 2014.
- 570 Gelencsér, A., May, B., Simpson, D., Sánchez-Ochoa, A., Kasper-Giebl, A., Puxbaum, H., Caseiro, A., Pio, C.A., Legrand, M.:  
571 Source apportionment of PM<sub>2.5</sub> organic aerosol over Europe: Primary/secondary, natural/anthropogenic, and  
572 fossil/biogenic origin, *J. Geophys. Res. Atmos.* 112, 1–12, <https://doi.org/10.1029/2006JD008094>, 2007.
- 573 He, Q.F., Ding, X., Fu, X.X., Zhang, Y.Q., Wang, J.Q., Liu, Y.X., Tang, M.J., Wang, X.M., Rudich, Y., Secondary organic  
574 aerosol formation from isoprene epoxides in the Pearl River Delta, South China: IEPOX- and HMML-derived tracers,  
575 *J. Geophys. Res. Atmos.*, 123, 6999–7012, <https://doi.org/10.1029/2017JD028242>, 2018.
- 576 He, X., Huang, X.H.H., Chow, K.S., Wang, Q., Zhang, T., Wu, D., Yu, J.Z.: Abundance and sources of phthalic acids, benzene-  
577 tricarboxylic acids, and phenolic acids in PM<sub>2.5</sub> at urban and suburban sites in Southern China, *ACS Earth Sp. Chem.*, 2,  
578 147–158, <https://doi.org/10.1021/acsearthspacechem.7b00131>, 2018.
- 579 Hildemann, L.M., Rogge, W.F., Cass, G.R., Mazurek, M.A., Simoneit, B.R.T.: Contribution of primary aerosol emissions from  
580 vegetation-derived sources to fine particle concentrations in Los Angeles, *J. Geophys. Res.*, 101, 19541,  
581 <https://doi.org/10.1029/95JD02136>, 1996.
- 582 Hofzumahaus, A., Rohrer, F., Lu, K., Bohn, B., Brauers, T., Chang, C.-C., Fuchs, H., Holland, F., Kita, K., Kondo, Y., Li, X.,  
583 Lou, S., Shao, M., Zeng, L., Wahner, A., Zhang, Y.: Amplified trace gas removal in the troposphere, *Science*, 324, 1702–  
584 1704, <https://doi.org/10.1126/science.1164566>, 2009.
- 585 Hu, D., Yu, J. Z.: Secondary organic aerosol tracers and malic acid in Hong Kong: Seasonal trends and origins, *Environ. Chem.*,  
586 10, 381–394, <https://doi.org/10.1071/EN13104>, 2013.
- 587 Hu, D., Bian, Q., Li, T.W.Y., Lau, A.K.H., Yu, J.Z.: Contributions of isoprene, monoterpenes, β-caryophyllene, and toluene to  
588 secondary organic aerosols in Hong Kong during the summer of 2006, *J. Geophys. Res. Atmos.*, 113,  
589 <https://doi.org/10.1029/2008JD010437>, 2008.
- 590 Hu, D., Bian, Q., Lau, A.K.H., Yu, J.Z.: Source apportioning of primary and secondary organic carbon in summer PM<sub>2.5</sub> in  
591 Hong Kong using positive matrix factorization of secondary and primary organic tracer data, *J. Geophys. Res. Atmos.*,  
592 115, 1–14, <https://doi.org/10.1029/2009JD012498>, 2010.
- 593 Huang, R.J., Zhang, Y., Bozzetti, C., Ho, K.F., Cao, J.J., Han, Y., Daellenbach, K.R., Slowik, J.G., Platt, S.M., Canonaco, F.,  
594 Zotter, P., Wolf, R., Pieber, S.M., Brun, E.A., Crippa, M., Ciarelli, G., Piazzalunga, A., Schwikowski, M., Abbazade,  
595 G., Schnelle-Kreis, J., Zimmermann, R., An, Z., Szidat, S., Baltensperger, U., El Haddad, I., Prevot, A.S.: High secondary  
596 aerosol contribution to particulate pollution during haze events in China, *Nature*, 514, 218–222,  
597 <https://doi.org/10.1038/nature13774>, 2014.
- 598 Jang, M., Czoschke, N.M., Lee, S., Kamens, R.M.: Heterogeneous atmospheric aerosol production by acid-catalyzed particle-  
599 phase reactions, *Science*, 298, 814–817, <https://doi.org/10.1126/science.1075798>, 2002.
- 600 Jaoui, M., Kleindienst, T.E., Lewandowski, M., Offenberg, J.H., Edney, E.O.: Identification and quantification of aerosol polar  
601 oxygenated compounds bearing carboxylic or hydroxyl groups. 2. Organic tracer compounds from monoterpenes,  
602 *Environ. Sci. Technol.*, 39, 5661–5673, <https://doi.org/10.1021/es048111b>, 2005.
- 603 Jokinen, T., Berndt, T., Makkonen, R., Kerminen, V.M., Junninen, H., Paasonen, P., Stratmann, F., Herrmann, H., Guenther,  
604 A.B., Worsnop, D.R., Kulmala, M., Ehn, M., Sipilä, M.: Production of extremely low volatile organic compounds from  
605 biogenic emissions: Measured yields and atmospheric implications, *Proc. Natl. Acad. Sci. U. S. A.*, 112, 7123–7128,  
606 <https://doi.org/10.1073/pnas.1423977112>, 2015.
- 607 Kanakidou, M., Seinfeld, J.H., Pandis, S.N., Barnes, I., Dentener, F.J., Facchini, M.C., Van Dingenen, R., Ervens, B., Nenes,



- 608 A., Nielsen, C.J., Swietlicki, E., Putaud, J.P., Balkanski, Y., Fuzzi, S., Horth, J., Moortgat, G.K., Winterhalter, R., Myhre,  
609 C.E.L., Tsigaridis, K., Vignati, E., Stephanou, E.G., Wilson, J.: Organic aerosol and global climate modelling: a review,  
610 *Atmos. Chem. Phys.*, 5, 1053–1123, <https://doi.org/10.5194/acp-5-1053-2005>, 2005.
- 611 Kautzman, K.E., Surratt, J.D., Chan, M.N., Chan, A.W.H., Hersey, S.P., Chhabra, P.S., Dalleska, N.F., Wennberg, P.O., Flagan,  
612 R.C., Seinfeld, J.H.: Chemical composition of gas- and aerosol-phase products from the photooxidation of naphthalene,  
613 *J. Phys. Chem. A*, 114, 913–934, <https://doi.org/10.1021/jp908530s>, 2010.
- 614 Kenseth, C.M., Huang, Y., Zhao, R., Dalleska, N.F., Caleb Hethcox, J., Stoltz, B.M., Seinfeld, J.H.: Synergistic O<sub>3</sub>+OH  
615 oxidation pathway to extremely low-volatility dimers revealed in β-pinene secondary organic aerosol, *Proc. Natl. Acad.*  
616 *Sci. U. S. A.*, 115, 8301–8306, <https://doi.org/10.1073/pnas.1804671115>, 2018.
- 617 Kitanovski, Z., Grgić, I., Vermeylen, R., Claeys, M., Maenhaut, W.: Liquid chromatography tandem mass spectrometry method  
618 for characterization of monoaromatic nitro-compounds in atmospheric particulate matter, *J. Chromatogr. A*, 1268, 35–  
619 43, <https://doi.org/10.1016/j.chroma.2012.10.021>, 2012.
- 620 Kleindienst, T.E., Jaoui, M., Lewandowski, M., Offenberg, J.H., Lewis, C.W., Bhave, P. V., Edney, E.O.: Estimates of the  
621 contributions of biogenic and anthropogenic hydrocarbons to secondary organic aerosol at a southeastern US location,  
622 *Atmos. Environ.*, 41, 8288–8300, <https://doi.org/10.1016/j.atmosenv.2007.06.045>, 2007.
- 623 Kleindienst, T.E., Lewandowski, M., Offenberg, J.H., Jaoui, M., Edney, E.O.: The formation of secondary organic aerosol  
624 from the isoprene + OH reaction in the absence of NO<sub>x</sub>, *Atmos. Chem. Phys.*, 9, 6541–6558, [https://doi.org/10.5194/acp-](https://doi.org/10.5194/acp-9-6541-2009)  
625 [9-6541-2009](https://doi.org/10.5194/acp-9-6541-2009), 2009.
- 626 Kleindienst, T.E., Jaoui, M., Lewandowski, M., Offenberg, J.H., Docherty, K.S.: The formation of SOA and chemical tracer  
627 compounds from the photo-oxidation of naphthalene and its methyl analogs in the presence and absence of nitrogen  
628 oxides, *Atmos. Chem. Phys.*, 12, 8711–8726, <https://doi.org/10.5194/acp-12-8711-2012>, 2012.
- 629 Lee, A., Goldstein, A.H., Keywood, M.D., Gao, S., Varutbangkul, V., Bahreini, R., Ng, N.L., Flagan, R.C., Seinfeld, J.H.: Gas-  
630 phase products and secondary aerosol yields from the ozonolysis of ten different terpenes, *J. Geophys. Res. Atmos.*, 111,  
631 1–18, <https://doi.org/10.1029/2005JD006437>, 2006a.
- 632 Lee, A., Goldstein, A.H., Kroll, J.H., Ng, N.L., Varutbangkul, V., Flagan, R.C., Seinfeld, J.H.: Gas-phase products and  
633 secondary aerosol yields from the photo-oxidation of 16 different terpenes, *J. Geophys. Res. Atmos.*, 111, D17305,  
634 <https://doi.org/10.1029/2006JD007050>, 2006b.
- 635 Lewandowski, M., Jaoui, M., Offenberg, J.H., Kleindienst, T.E., Edney, E.O., Sheesley, R. J., Schauer, J.J.: Primary and  
636 secondary contributions to ambient PM in the midwestern united states, *Environ. Sci. Technol.*, 42, 3303–3309,  
637 <https://doi.org/10.1021/es0720412>, 2008.
- 638 Lin, Y.-H., Zhang, Z., Docherty, K.S., Zhang, H., Budisulistiorini, S.H., Rubitschun, C.L., Shaw, S.L., Knipping, E.M.,  
639 Edgerton, E.S., Kleindienst, T.E., Gold, A., Surratt, J.D.: Isoprene epoxydiols as precursors to secondary organic aerosol  
640 formation: Acid-catalyzed reactive uptake studies with authentic compounds, *Environ. Sci. Technol.*, 46, 250–258,  
641 <https://doi.org/10.1021/es202554c>, 2012.
- 642 Lin, Y.-H., Zhang, H., Pye, H.O.T., Zhang, Z., Marth, W.J., Park, S., Arashiro, M., Cui, T., Budisulistiorini, S.H., Sexton, K.G.,  
643 Vizuete, W., Xie, Y., Luecken, D.J., Piletic, I.R., Edney, E.O., Bartolotti, L.J., Gold, A., Surratt, J.D.: Epoxide as a  
644 precursor to secondary organic aerosol formation from isoprene photo-oxidation in the presence of nitrogen oxides, *Proc.*  
645 *Natl. Acad. Sci. U. S. A.*, 110, 6718–6723, <https://doi.org/10.1073/pnas.1221150110>, 2013.
- 646 Lu, X., Fung, J.: Source apportionment of sulfate and nitrate over the Pearl River Delta Region in China, *Atmosphere*, 7, 98,  
647 <https://doi.org/10.3390/atmos7080098>, 2016.
- 648 Ma, Y., Cheng, Y., Qiu, X., Lin, Y., Cao, J., Hu, D.: A quantitative assessment of source contributions to fine particulate matter  
649 (PM<sub>2.5</sub>)-bound polycyclic aromatic hydrocarbons (PAHs) and their nitrated and hydroxylated derivatives in Hong Kong,  
650 *Environ. Pollut.*, 219, 742–749, <https://doi.org/10.1016/j.envpol.2016.07.034>, 2016.



- 651 Ma, Y., Cheng, Y., Qiu, X., Cao, G., Fang, Y., Wang, J., Zhu, T., Yu, J., Hu, D.: Sources and oxidative potential of water-soluble  
652 humic-like substances (HULIS<sub>WS</sub>) in fine particulate matter (PM<sub>2.5</sub>) in Beijing, *Atmos. Chem. Phys.*, 18, 5607–5617,  
653 <https://doi.org/10.5194/acp-18-5607-2018>, 2018.
- 654 Ma, Y., Cheng, Y., Qiu, X., Cao, G., Kuang, B., Yu, J.Z., Hu, D.: Optical properties, source apportionment and redox activity  
655 of humic-like substances (HULIS) in airborne fine particulates in Hong Kong, *Environ. Pollut.*, 255, 113087,  
656 <https://doi.org/10.1016/j.envpol.2019.113087>, 2019.
- 657 Mancilla, Y., Herckes, P., Fraser, M.P., Mendoza, A.: Secondary organic aerosol contributions to PM<sub>2.5</sub> in Monterrey, Mexico:  
658 Temporal and seasonal variation, *Atmos. Res.*, 153, 348–359, <https://doi.org/10.1016/j.atmosres.2014.09.009>, 2015.
- 659 Minerath, E. C., Casale, M. T., Elrod, M. J.: Kinetics feasibility study of alcohol sulfate esterification reactions in tropospheric  
660 aerosols, *Environ. Sci. Technol.*, 42, 4410–4415, <https://doi.org/10.1021/es8004333>, 2008.
- 661 Ng, N.L., Kwan, A.J., Surratt, J.D., Chan, A.W.H., Chhabra, P.S., Sorooshian, A., Pye, H.O.T., Crouse, J.D., Wennberg, P.O.,  
662 Flagan, R.C., Seinfeld, J.H.: Secondary organic aerosol (SOA) formation from reaction of isoprene with nitrate radicals  
663 (NO<sub>3</sub>), *Atmos. Chem. Phys.*, 8, 4117–4140, <https://doi.org/10.5194/acp-8-4117-2008>, 2008.
- 664 Nguyen, T.B., Bates, K.H., Crouse, J.D., Schwantes, R.H., Zhang, X., Kjaergaard, H.G., Surratt, J.D., Lin, P., Laskin, A.,  
665 Seinfeld, J.H., Wennberg, P.O.: Mechanism of the hydroxyl radical oxidation of methacryloyl peroxyxynitrate (MPAN)  
666 and its pathway toward secondary organic aerosol formation in the atmosphere, *Phys. Chem. Chem. Phys.*, 17, 17914–  
667 17926, <https://doi.org/10.1039/c5cp02001h>, 2015.
- 668 Offenberg, J. H., Lewis, C. W., Lewandowski, M., Jaoui, M., Kleindienst, T. E., Edney, E. O.: Contributions of toluene and  $\alpha$ -  
669 pinene to SOA formed in an irradiated toluene/ $\alpha$ -pinene/NO<sub>x</sub>/air mixture: comparison of results using <sup>14</sup>C content and  
670 SOA organic tracer methods, *Environ. Sci. Technol.*, 41, 3972–3976, <https://doi.org/10.1021/es070089>, 2007.
- 671 Rattanavaraha, W., Chu, K., Budisulistiorini, S.H., Riva, M., Lin, Y.H., Edgerton, E.S., Baumann, K., Shaw, S.L., Guo, H.,  
672 King, L., Weber, R.J., Neff, M.E., Stone, E.A., Offenberg, J.H., Zhang, Z., Gold, A., Surratt, J.D.: Assessing the impact  
673 of anthropogenic pollution on isoprene-derived secondary organic aerosol formation in PM<sub>2.5</sub> collected from the  
674 Birmingham, Alabama, ground site during the 2013 Southern Oxidant and Aerosol Study, *Atmos. Chem. Phys.*, 16,  
675 4897–4914, <https://doi.org/10.5194/acp-16-4897-2016>, 2016.
- 676 Riedel, T.P., Lin, Y.H., Budisulistiorini, S.H., Gaston, C.J., Thornton, J.A., Zhang, Z., Vizuete, W., Gold, A., Surratt, J.D.:  
677 Heterogeneous reactions of isoprene-derived epoxides: Reaction probabilities and molar secondary organic aerosol yield  
678 estimates, *Environ. Sci. Technol. Lett.*, 2, 38–42, <https://doi.org/10.1021/ez500406f>, 2015.
- 679 Riva, M., Tomaz, S., Cui, T., Lin, Y.H., Perraudin, E., Gold, A., Stone, E.A., Villenave, E., Surratt, J.D.: Evidence for an  
680 unrecognized secondary anthropogenic source of organosulfates and sulfonates: Gas-phase oxidation of polycyclic  
681 aromatic hydrocarbons in the presence of sulfate aerosol, *Environ. Sci. Technol.*, 49, 6654–6664,  
682 <https://doi.org/10.1021/acs.est.5b00836>, 2015.
- 683 Roberts, J.M., Bertman, S.B.: The thermal decomposition of peroxyacetic nitric anhydride (PAN) and peroxyacetic nitric  
684 anhydride (MPAN), *Int. J. Chem. Kinet.*, 24, 297–307, <https://doi.org/10.1002/kin.550240307>, 1992.
- 685 Rollins, A.W., Pusede, S., Wooldridge, P., Min, K.-E., Gentner, D. R., Goldstein, A.H., Liu, S., Day, D. A., Russell, L. M.,  
686 Rubitschun, C. L., Surratt, J. D., Cohen, R.C.: Gas particle partitioning of total alkyl nitrates observed with TD-LIF in  
687 Bakersfield, *J. Geophys. Res. Atmos.*, 118, 6651–6662, <https://doi.org/10.1002/jgrd.50522>, 2013.
- 688 Sang, X.F., Chan, C.Y., Engling, G., Chan, L.Y., Wang, X.M., Zhang, Y.N., Shi, S., Zhang, Z.S., Zhang, T., Hu, M.:  
689 Levoglucosan enhancement in ambient aerosol during springtime transport events of biomass burning smoke to  
690 Southeast China, *Tellus B*, 63, 129–139, <https://doi.org/10.1111/j.1600-0889.2010.00515.x>, 2011.
- 691 Schauer, J.J., Kleeman, M.J., Cass, G.R., Simoneit, B.R.T.: Measurement of emissions from air pollution sources. 3. C<sub>1</sub>–C<sub>29</sub>  
692 organic compounds from fireplace combustion of wood, *Environ. Sci. Technol.*, 35, 1716–1728,  
693 <https://doi.org/10.1021/es001331e>, 2001.

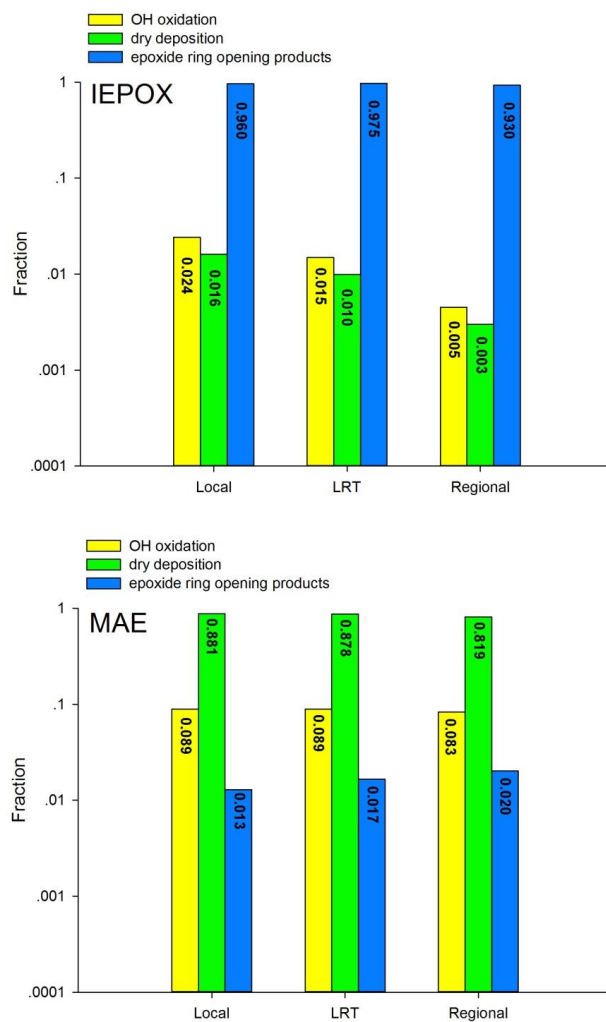


- 694 Schauer, J.J., Rogge, W.F., Hildemann, L.M., Mazurek, M.A., Cass, G.R., Simoneit, B.R.T.: Source apportionment of airborne  
695 particulate matter using organic compounds as tracers, *Atmos. Environ.*, 41, 241–259,  
696 <https://doi.org/10.1016/j.atmosenv.2007.10.069>, 2007.
- 697 Simoneit, B.R.T.: A review of biomarker compounds as source indicators and tracers for air pollution, *Environ. Sci. Pollut.*  
698 *Res.*, 6, 159–169, <https://doi.org/10.1007/BF02987621>, 1999.
- 699 Simoneit, B.R.T., Medeiros, P.M., Didyk, B.M.: Combustion products of plastics as indicators for refuse burning in the  
700 atmosphere, *Environ. Sci. Technol.*, 39, 6961–6970, <https://doi.org/10.1021/es050767x>, 2005.
- 701 Surratt, J.D., Chan, A.W.H., Eddingsaas, N.C., Chan, M., Loza, C.L., Kwan, A.J., Hersey, S.P., Flagan, R.C., Wennberg, P.O.,  
702 Seinfeld, J.H.: Reactive intermediates revealed in secondary organic aerosol formation from isoprene, *Proc. Natl. Acad.*  
703 *Sci. U. S. A.*, 107, 6640–6645, <https://doi.org/10.1073/pnas.0911114107>, 2010.
- 704 Tsui, J.K.Y., Guenther, A., Yip, W.K., Chen, F.: A biogenic volatile organic compound emission inventory for Hong Kong,  
705 *Atmos. Environ.*, 43, 6442–6448, <https://doi.org/10.1016/j.atmosenv.2008.01.027>, 2009.
- 706 Van Dingenen, R., Raes, F., Putaud, J.P., Baltensperger, U., Charron, A., Facchini, M.C., Decesari, S., Fuzzi, S., Gehrig, R.,  
707 Hansson, H.C., Harrison, R.M., Hüglin, C., Jones, A.M., Laj, P., Lorbeer, G., Maenhaut, W., Palmgren, F., Querol, X.,  
708 Rodriguez, S., Schneider, J., Ten Brink, H., Tunved, P., Tørseth, K., Wehner, B., Weingartner, E., Wiedensohler, A.,  
709 Wählin, P.: A European aerosol phenomenology-1: Physical characteristics of particulate matter at kerbside, urban, rural  
710 and background sites in Europe, *Atmos. Environ.*, 38, 2561–2577, <https://doi.org/10.1016/j.atmosenv.2004.01.040>, 2004.
- 711 Viana, M., Amato, F., Alastuey, A., Querol, X., Moreno, T., Dos Santos, S.G., Hecce, M.D., Fernández-Patier, R.: Chemical  
712 tracers of particulate emissions from commercial shipping, *Environ. Sci. Technol.*, 43, 7472–7477,  
713 <https://doi.org/10.1021/es901558t>, 2009.
- 714 Vione, D., Maurino, V., Minero, C., Pelizzetti, E.: Phenol photonitration upon UV irradiation of nitrite in aqueous solution II:  
715 Effects of pH and TiO<sub>2</sub>, *Chemosphere*, 45, 903–910, [https://doi.org/10.1016/S0045-6535\(01\)00036-4](https://doi.org/10.1016/S0045-6535(01)00036-4), 2001.
- 716 Wang, G., Zhang, R., Gomez, M.E., Yang, L., Zamora, M.L., Hu, M., Lin, Y., Peng, J., Guo, S., Meng, J., Li, J., Cheng, C.,  
717 Hu, T., Ren, Y., Wang, Y.Y., Gao, J., Cao, J., An, Z., Zhou, W., Li, G., Wang, J., Tian, P., Marrero-Ortiz, W., Secrest, J.,  
718 Du, Z., Zheng, J., Shang, D., Zeng, L., Shao, M., Wang, W., Huang, Y., Wang, Y.Y., Zhu, Y., Li, Y., Hu, J., Pan, B., Cai,  
719 L., Cheng, Y., Ji, Y., Zhang, F., Rosenfeld, D., Liss, P.S., Duce, R.A., Kolb, C.E., Molina, M.J., Peng, J., Duan, L., Ji, Y.,  
720 Marrero-Ortiz, W., An, Z., Huang, R., Zhang, R., Tie, X., Li, G., Cao, J.: Persistent sulfate formation from London Fog  
721 to Chinese haze, *Proc. Natl. Acad. Sci. U. S. A.*, 113, 13630–13635, <https://doi.org/10.1073/pnas.1616540113>, 2016.
- 722 Worton, D.R., Surratt, J.D., LaFranchi, B.W., Chan, A.W.H., Zhao, Y., Weber, R.J., Park, J.-H., Gilman, J.B., De Gouw, J.,  
723 Park, C., Schade, G., Beaver, M.R., St. Clair, J., Crounse, J.D., Wennberg, P., Wolfe, G.M., Harrold, S., Thornton, J.,  
724 Farmer, D., Docherty, K.S., Cubison, M., Jimenez, J.L., Frossard, A., Russell, L.M., Kristensen, K., Glasius, M., Mao,  
725 J., Ren, X., Brune, B., Browne, E.C., Pusede, S., Cohen, R.C., Seinfeld, J.H., Goldstein, A.H.: Observational insights  
726 into high- and low-NO<sub>x</sub> aerosol formation from isoprene, *Environ. Sci. Technol.*, 47, 11403–11413,  
727 <https://doi.org/10.1021/es4011064>, 2013.
- 728 Xie, B., Fung, J. C. H., Chan, A., Lau, A.: Evaluation of nonlocal and local planetary boundary layer schemes in the WRF  
729 model, *J. Geophys. Res. Atmos.*, 117, D12103, <https://doi.org/10.1029/2011JD017080>, 2012.
- 730 Xu, L., Guo, H., Boyd, C.M., Klein, M., Bougiatioti, A., Cerully, K.M., Hite, J.R., Isaacman-VanWertz, G., Kreisberg, N.M.,  
731 Knote, C., Olson, K., Koss, A., Goldstein, A.H., Hering, S. V., de Gouw, J., Baumann, K., Lee, S.-H., Nenes, A., Weber,  
732 R.J., Ng, N.L.: Effects of anthropogenic emissions on aerosol formation from isoprene and monoterpenes in the  
733 southeastern United States, *Proc. Natl. Acad. Sci. U. S. A.*, 112, 37–42, <https://doi.org/10.1073/pnas.1417609112>, 2015.
- 734 Yu, J.Z., Huang, X.-F., Xu, J., Hu, M.: When aerosol sulfate goes up, so does oxalate: Implication for the formation  
735 mechanisms of oxalate, *Environ. Sci. Technol.*, 39, 128–133, <https://doi.org/10.1021/es049559f>, 2005.
- 736 Yu, L., Smith, J., Laskin, A., Anastasio, C., Laskin, J., Zhang, Q.: Chemical characterization of SOA formed from aqueous-



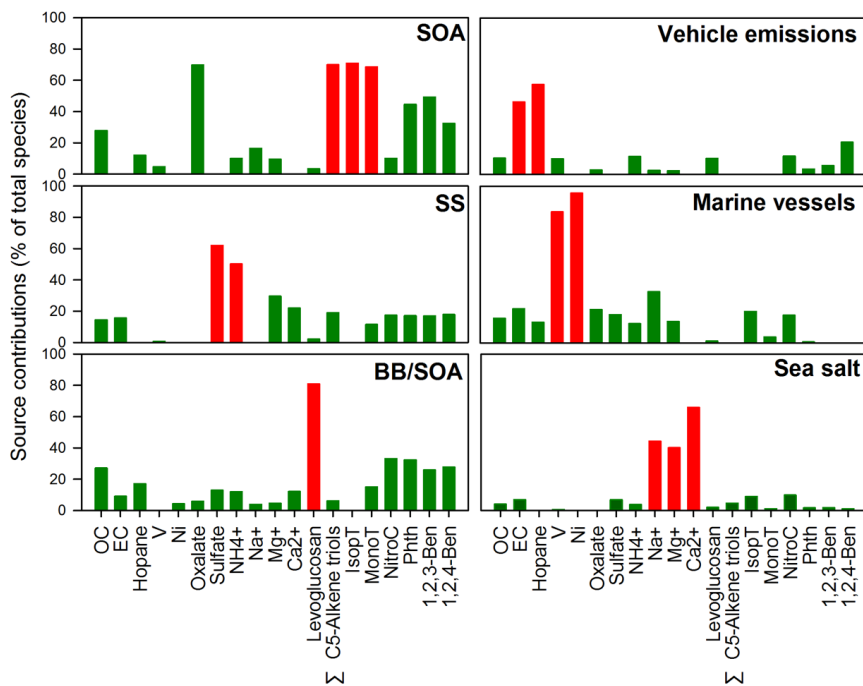


- 737 phase reactions of phenols with the triplet excited state of carbonyl and hydroxyl radical, *Atmos. Chem. Phys.*, 14,  
738 13801–13816, <https://doi.org/10.5194/acp-14-13801-2014>, 2014.
- 739 Yuan, Z.B., Yu, J.Z., Lau, A.K.H., Louie, P.K.K., Fung, J.C.H.: Application of positive matrix factorization in estimating  
740 aerosol secondary organic carbon in Hong Kong and its relationship with secondary sulfate, *Atmos. Chem. Phys.*, 6, 25–  
741 34, <https://doi.org/10.5194/acp-6-25-2006>, 2006.
- 742 Worton, D.R., Surratt, J.D., LaFranchi, B.W., Chan, A.W.H., Zhao, Y., Weber, R.J., Park, J.-H., Gilman, J.B., De Gouw, J.,  
743 Park, C., Schade, G., Beaver, M.R., StClair, J., Crouse, J.D., Wennberg, P., Wolfe, G.M., Harrold, S., Thornton, J.,  
744 Farmer, D., Docherty, K.S., Cubison, M., Jimenez, J.L., Frossard, A. a, Russell, L.M., Kristensen, K., Glasius, M., Mao,  
745 J., Ren, X., Brune, B., Browne, E.C., Pusede, S., Cohen, R.C., Seinfeld, J.H., Goldstein, A.H.: Observational insights  
746 into high- and low-NO<sub>x</sub> aerosol formation from isoprene, *Environ. Sci. Technol.*, 47, 11403–11413,  
747 <https://doi.org/10.1021/es4011064>, 2013.
- 748 Zhang, H., Yee, L.D., Lee, B.H., Curtis, M.P., Worton, D.R., Isaacman-VanWertz, G., Offenberg, J.H., Lewandowski, M.,  
749 Kleindienst, T.E., Beaver, M.R., Holder, A.L., Lonneman, W.A., Docherty, K.S., Jaoui, M., Pye, H.O.T., Hu, W., Day,  
750 D.A., Campuzano-Jost, P., Jimenez, J.L., Guo, H., Weber, R.J., De Gouw, J., Koss, A.R., Edgerton, E.S., Brune, W.,  
751 Mohr, C., Lopez-Hilfiker, F.D., Lutz, A., Kreisberg, N.M., Spielman, S.R., Hering, S. V., Wilson, K.R., Thornton, J.A.,  
752 Goldstein, A.H.: Monoterpenes are the largest source of summertime organic aerosol in the southeastern United States,  
753 *Proc. Natl. Acad. Sci. U. S. A.*, 115, 2038–2043, <https://doi.org/10.1073/pnas.1717513115>, 2018.
- 754 Zhang, Q., Jimenez, J.L., Canagaratna, M.R., Allan, J.D., Coe, H., Ulbrich, I., Alfarra, M.R., Takami, A., Middlebrook, A.M.,  
755 Sun, Y.L., Dzepina, K., Dunlea, E., Docherty, K., DeCarlo, P.F., Salcedo, D., Onasch, T., Jayne, J.T., Miyoshi, T.,  
756 Shimono, A., Hatakeyama, S., Takegawa, N., Kondo, Y., Schneider, J., Drewnick, F., Borrmann, S., Weimer, S.,  
757 Demerjian, K., Williams, P., Bower, K., Bahreini, R., Cottrell, L., Griffin, R.J., Rautiainen, J., Sun, J.Y., Zhang, Y.M.,  
758 Worsnop, D.R.: Ubiquity and dominance of oxygenated species in organic aerosols in anthropogenically-influenced  
759 Northern Hemisphere midlatitudes, *Geophys. Res. Lett.*, 34, 1–6, <https://doi.org/10.1029/2007GL029979>, 2007.
- 760 Zhang, T., Claeys, M., Cachier, H., Dong, S., Wang, W., Maenhaut, W., Liu, X.: Identification and estimation of the biomass  
761 burning contribution to Beijing aerosol using levoglucosan as a molecular marker, *Atmos. Environ.*, 42, 7013–7021,  
762 <https://doi.org/10.1016/j.atmosenv.2008.04.050>, 2008.
- 763 Zhang, Y. X., Shao, M., Zhang, Y.H., Zeng, L.M., He, L.Y., Zhu, B., Wei, Y.J., Zhu, X.L.: Source profiles of particulate organic  
764 matters emitted from cereal straw burnings, *J. Environ. Sci.*, 19, 167–175, [https://doi.org/10.1016/S1001-0742\(07\)60027-8](https://doi.org/10.1016/S1001-0742(07)60027-8), 2007.
- 766 Zheng, M., Salmon, L.G., Schauer, J.J., Zeng, L., Kiang, C.S., Zhang, Y., Cass, G.R.: Seasonal trends in PM<sub>2.5</sub> source  
767 contributions in Beijing, China, *Atmos. Environ.*, 39, 3967–3976, <https://doi.org/10.1016/j.atmosenv.2005.03.036>, 2005.
- 768 Zheng, M., Zhao, X., Cheng, Y., Yan, C., Shi, W., Zhang, X., Weber, R.J., Schauer, J.J., Wang, X., Edgerton, E.S.: Sources of  
769 primary and secondary organic aerosol and their diurnal variations, *J. Hazard. Mater.*, 264, 536–544,  
770 <https://doi.org/10.1016/j.jhazmat.2013.10.047>, 2014.



771

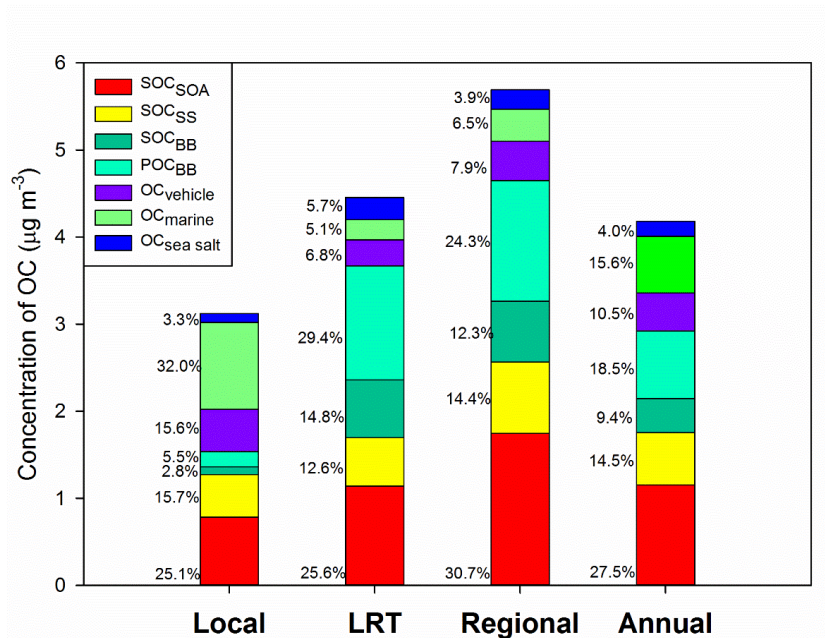
772 Figure 1: Comparison of three degradation processes for IEPOX and MAE under the three synoptic conditions



773

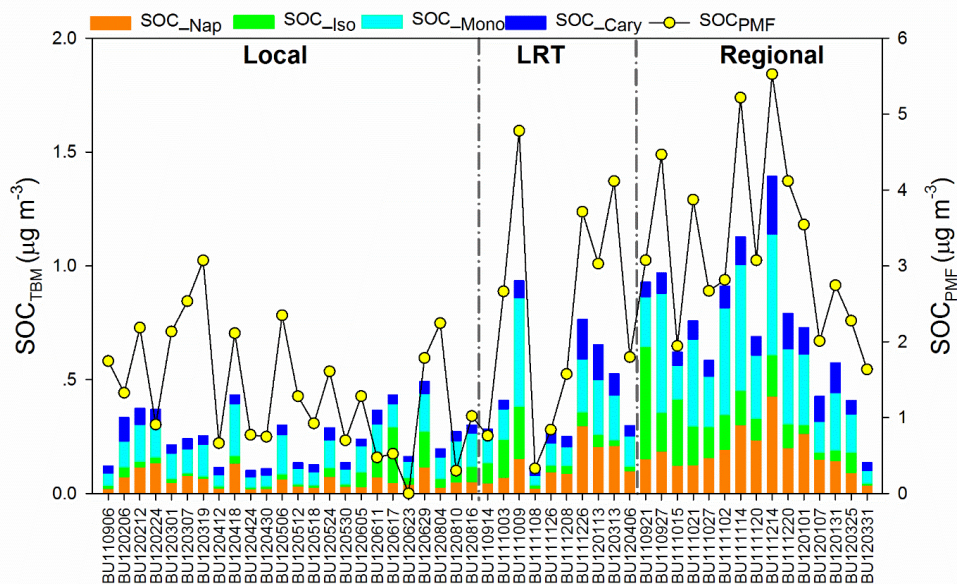
774 Figure 2: PMF-resolved source contributions (% of total species) to ambient PM<sub>2.5</sub> samples collected in Hong Kong. Red  
 775 column: chemical markers for source identification.

776



777

778 Figure 3: Source-specific contributions to OC under different meteorological conditions. OC<sub>BB</sub> was split into POC<sub>BB</sub> and  
 779 SOC<sub>BB</sub>.



780

781 Figure 4: Temporal variations of SOC<sub>PMF</sub> and SOC<sub>TBM</sub>.



782 Table 1: Concentrations of 15 SOA tracers, 25 polar organic compounds, and nine inorganic ions in PM<sub>2.5</sub> collected in Hong  
 783 Kong under three meteorological conditions.

	Local (N=24) Average	Range	Long regional (N=10) Average	transport Range	Regional (N=15) Average	Range
<i>Tracers for isoprene SOA (ng m<sup>-3</sup>)</i>						
2-Methylglyceric acid	0.56±0.31	0.22-1.42	1.28±0.86	0.29-2.61	2.36±1.75	0.02-6.42
2-Methylthreitol	2.34±3.95	0.33-18.79	2.88±2.97	0.57-9.60	6.23±5.69	0.35-23.37
2-Methylerythritol	7.06±13.95	0.54-64.67	6.94±7.81	1.08-23.58	13.49±12.23	0.48-47.62
cis-2-Methyl-1,3,4-trihydroxy-1-butene	0.87±1.25	0.15-6.06	2.00±2.56	0.33-8.62	5.78±4.57	0.22-17.19
3-Methyl-2,3,4-trihydroxy-1-butene	0.52±0.49	0.15-2.00	1.03±1.17	0.23-4.08	2.40±1.91	0.18-7.31
trans-2-Methyl-1,3,4-trihydroxy-1-butene	1.28±1.25	0.15-5.08	5.25±5.59	0.48-18.68	10.52±8.19	0.37-25.23
3-MeTHF-3,4-diols	0.18±0.06	0.15-0.34	0.21±0.07	0.15-0.32	0.29±0.12	0.15-0.60
∑C5-Alkene triols	2.68±2.52	0.45-8.89	8.27±8.92	1.20-31.37	18.71±13.14	0.78-40.08
∑Isoprene tracers (exclude triols)	10.06±18.09	1.22-84.87	11.23±11.18	1.93-35.70	22.32±18.94	1.17-77.09
∑Isoprene tracers	12.74±20.13	1.67-93.41	19.51±19.41	3.14-67.07	41.03±29.71	1.95-117.17
<i>Tracers for monoterpenes SOA (ng m<sup>-3</sup>)</i>						
3-Hydroxyglutaric acid	3.40±2.09	0.72-9.14	6.11±5.42	0.66-19.15	11.53±6.27	1.35-22.04
3-Hydroxy-4,4-dimethylglutaric acid	0.53±0.12	0.42-0.93	0.71±0.30	0.43-1.39	0.91±0.28	0.41-1.39
3-Methyl-1,2,3-butanetricarboxylic acid	0.59±0.19	0.40-1.18	0.84±0.39	0.45-1.76	1.28±0.52	0.42-2.14
3-Isopropylpentanedioic acid	1.07±0.38	0.55-1.85	1.52±0.86	0.51-3.46	2.57±1.52	0.61-4.86
3-Acetyl pentanedioic acid	0.82±0.23	0.45-1.19	1.13±0.55	0.49-2.42	1.71±0.87	0.54-3.20
∑ Monoterpenes tracers	6.41±2.75	2.63-13.49	10.31±7.33	2.54-28.17	18.00±9.28	3.33-32.57
<i>Tracers for β-caryophyllene SOA (ng m<sup>-3</sup>)</i>						
β-Caryophyllinic acid	0.94±0.41	0.49-2.36	1.73±1.16	0.75-3.99	2.33±1.21	0.80-5.82
<i>Tracers for Naphthalene SOA (ng m<sup>-3</sup>)</i>						
Phthalic acid	2.26±1.38	0.80-5.17	4.97±3.30	0.92-11.41	7.16±3.61	1.41-16.42
<i>Dicarboxylic acids (ng m<sup>-3</sup>)</i>						
Succinic acid	2.10±1.63	0.65-6.23	4.56±4.80	0.80-14.18	5.27±3.43	0.68-12.19
Maleic acid	0.42±0.27	0.14-1.47	0.42±0.23	0.14-0.84	0.36±0.18	0.15-0.78
Malic acid	2.67±1.49	0.64-5.59	4.20±3.74	0.60-13.12	8.10±4.12	1.33-13.86
Glutaric acid	2.63±6.06	0.82-30.89	2.36±1.73	0.79-4.99	2.85±1.53	0.67-6.05
Citramalic acid	0.76±0.23	0.38-1.30	0.86±0.32	0.38-1.48	1.23±0.47	0.52-2.00
Terephthalic acid	9.28±7.49	2.16-31.86	30.21±27.20	3.58-79.61	36.89±23.84	3.77-79.25
Adipic acid	1.34±1.42	0.54-6.20	1.20±0.46	0.64-2.21	1.48±0.66	0.67-3.08
Pimelic acid	0.68±0.10	0.51-0.93	0.82±0.29	0.52-1.47	0.99±0.35	0.52-1.94
Oxalic acid (μg m <sup>-3</sup> )	0.35±0.20	0.11-0.86	0.38±0.23	0.09-0.72	0.54±0.21	0.29-0.94
<i>Saccharides (ng m<sup>-3</sup>)</i>						
Levogluconan	22.51±41.16	0.64-161.16	120.79±129.55	3.21-362.74	128.52±140.39	8.64-474.15
Meso-erythritol	0.11±0.10	0.03-0.43	0.29±0.25	0.03-0.74	0.44±0.28	0.07-1.22
Xylitol	0.29±0.11	0.21-0.69	0.50±0.28	0.23-1.02	0.52±0.22	0.22-1.03
Xylose	1.24±1.08	0.50-4.57	4.65±4.45	0.58-13.34	5.34±4.31	0.81-16.12
Galactose	1.82±2.02	0.37-9.97	3.31±1.97	1.09-7.08	3.51±1.71	1.02-6.84
Mannitol	0.16±0.04	0.12-0.26	0.21±0.07	0.13-0.37	0.23±0.07	0.13-0.37
Fructose	2.30±3.19	0.26-15.58	3.64±3.89	0.38-13.41	4.32±2.54	1.65-9.32
Galactosan	1.09±0.53	0.79-2.99	2.58±2.47	0.84-7.20	2.68±2.40	0.88-7.99
Sorbitol	1.45±0.37	1.14-2.54	1.55±0.28	1.21-1.96	1.70±0.40	1.31-2.62
Glucose	1.55±0.89	0.50-3.83	1.20±0.61	0.40-2.07	1.51±0.92	0.52-3.29
Sucrose	0.94±1.81	0.42-9.43	0.58±0.14	0.42-0.91	0.57±0.08	0.45-0.76
Arbitol	0.25±0.10	0.00-0.57	0.40±0.20	0.22-0.78	0.42±0.17	0.22-0.85
<i>Other compounds (ng m<sup>-3</sup>)</i>						



4-Nitrocatechol	0.90±0.12	0.78-1.35	1.30±0.62	0.84-2.75	1.55±0.83	0.85-4.00
Cholesterol	1.29±0.25	0.94-1.81	1.30±0.28	1.01-1.93	1.20±0.27	0.95-1.89
1,2,3-Benzenetricarboxylic Acid	1.23±0.67	0.47-2.46	2.25±1.34	0.63-4.70	3.97±2.54	0.54-9.50
1,2,4-Benzenetricarboxylic Acid	1.77±1.28	0.47-6.17	3.32±2.34	0.88-6.77	5.16±3.30	0.73-12.54
<i>Major ion (<math>\mu\text{g m}^{-3}</math>)</i>						
Sulfate	11.43±5.98	3.28-30.32	13.02±9.25	1.49-29.25	17.35±5.20	8.90-29.29
Nitrate	0.89±1.17	0.05-3.39	1.62±2.10	0.08-5.84	1.41±1.51	0.38-5.49
Chloride	0.18±0.17	0.06-0.77	0.17±0.15	0.07-0.45	0.14±0.09	0.07-0.40
Ammonia	2.05±0.91	0.47-4.12	2.26±1.48	0.30-4.36	2.99±0.72	1.82-4.69
Potassium	0.11±0.07	0.03-0.36	0.29±0.17	0.05-0.49	0.40±0.22	0.15-0.94
Magnesium	0.01±0.01	0.00-0.03	0.02±0.01	0.00-0.04	0.02±0.01	0.00-0.04
Calcium	0.03±0.03	0.00-0.13	0.08±0.07	0.02-0.23	0.08±0.04	0.02-0.15
Sodium	0.09±0.09	0.01-0.40	0.16±0.14	0.03-0.52	0.14±0.06	0.08-0.30

784



785 Table 2: PMF and TBM-resolved OCs, concentrations of gas pollutants, PM<sub>2.5</sub>, EC, OC, and major aerosol characteristics  
 786 under different meteorological conditions.

	Local (N=24)		Long regional transport (N=10)		Regional (N=15)		Annual (N=49)	
	Average	Range	Average	Range	Average	Range	Average	Range
PM <sub>2.5</sub> (µg m <sup>-3</sup> )	24.11±9.99	10.04-49.28	32.23±14.81	7.63-50.68	38.5±10.48	26.20-65.28	30.17±12.72	7.63-65.28
EC (µgC m <sup>-3</sup> )	1.02±0.57	0.47-2.75	0.85±0.60	0.14-2.10	1.14±0.45	0.50-2.12	1.02±0.54	0.14-2.75
OC <sub>measured</sub>	2.94±1.11	1.61-5.75	4.16±2.53	1.25-8.53	6.15±2.51	3.21-12.97	4.18±2.37	1.25-12.97
	<i>PMF apportioned OC (µgC m<sup>-3</sup>)</i>							
SOC <sub>SOA</sub>	0.78±0.65	0.00-2.27	1.14±0.82	0.18-2.72	1.75±0.75	0.65-3.29	1.15±0.82	0.00-3.29
SOC <sub>SS</sub>	0.49±0.37	0.00-1.74	0.56±0.67	0.00-1.81	0.82±0.38	0.24-1.65	0.60±0.46	0.00-1.81
OC <sub>BB</sub> (POC <sub>BB</sub> +SOC <sub>BB</sub> )	0.26±0.63	0.00-2.34	1.97±2.26	0.00-6.34	2.08±2.63	0.00-8.96	1.17±1.99	0.00-8.96
OC <sub>Vehicle</sub>	0.49±0.46	0.00-2.07	0.30±0.42	0.00-1.26	0.45±0.36	0.01-1.26	0.44±0.42	0.00-2.07
OC <sub>Marine</sub>	1.00±0.63	0.04-2.97	0.23±0.19	0.00-0.51	0.37±0.21	0.08-0.71	0.65±0.18	0.00-2.97
OC <sub>Sea salt</sub>	0.10±0.11	0.00-0.53	0.25±0.33	0.00-1.13	0.22±0.16	0.00-0.62	0.17±0.19	0.00-1.13
SOC <sub>BB</sub>	0.09±0.21	0.00-0.79	0.66±0.76	0.00-2.13	0.70±0.88	0.00-3.01	0.39±0.67	0.00-3.01
SOC <sub>PMF</sub>	1.36±0.81	0.00-3.07	2.36±1.54	0.33-4.78	3.27±1.18	1.63-5.53	2.15±1.37	0.00-5.53
SOC <sub>PMF</sub> /OC (%)	43.0±16.8%	0.0%-66.5%	52.3±21.1%	30.0%-85.3%	60.2±13.7%	36.2%-78.8%	50.2±18.2%	0.0%-85.3%
	<i>Tracer based method estimated OC (µgC m<sup>-3</sup>)</i>							
SOC <sub>Iso</sub>	0.04±0.06	0.01-0.24	0.07±0.07	0.01-0.23	0.14±0.12	0.01-0.49	0.08±0.09	0.01-0.49
SOC <sub>Mono</sub>	0.14±0.06	0.06-0.29	0.22±0.16	0.05-0.60	0.38±0.20	0.07-0.69	0.23±0.17	0.05-0.69
SOC <sub>Cary</sub>	0.04±0.02	0.02-0.10	0.08±0.05	0.03-0.17	0.10±0.05	0.03-0.25	0.07±0.05	0.02-0.25
SOC <sub>Nap</sub>	0.06±0.04	0.02-0.13	0.13±0.09	0.02-0.30	0.19±0.09	0.04-0.43	0.11±0.09	0.02-0.43
SOC <sub>TBM</sub>	0.28±0.13	0.11-0.53	0.50±0.29	0.12-1.06	0.81±0.35	0.15-1.53	0.49±0.34	0.11-1.53
SOC <sub>TBM</sub> /OC	10.2±5.1%	3.8%-22.7%	13.0±4.6%	5.3%-20.7%	13.4±4.3%	4.7%-19.6%	11.8±4.9%	3.8%-22.7%
	<i>Gas Pollutants and other aerosol characteristics</i>							
O <sub>3_</sub> average (ppb)	11.61±7.3	2.93-32.12	13.96±7.94	2.86-26.92	20.64±8.74	2.88-31.84	14.85±8.69	2.86-32.12
NO <sub>2_</sub> average (ppb)	34.56±10.66	16.7-54.32	34.59±7.62	21.74-42.85	42.98±7.10	32.72-60.37	37.15±9.76	16.70-60.37
SO <sub>2_</sub> average (µg m <sup>-3</sup> )	4.14±2.92	0.7-10.38	3.81±1.88	2.23-7.30	5.38±2.24	2.96-10.45	4.45±2.57	0.70-10.45
O <sub>x</sub> (µg m <sup>-3</sup> )	87.45±26.26	49.72-138.49	93.18±21.37	61.66-125.79	122.39±17.70	69.54-145.90	99.31±27.42	49.72-145.90
p[NO <sub>3</sub> ] (ppb h <sup>-1</sup> )	1.25±0.96	0.30-4.17	1.36±0.94	0.31-3.29	2.45±1.02	0.23-3.76	1.64±1.10	0.23-4.17
NO <sub>3_</sub> average (ppb)	0.05±0.04	0.01-0.18	0.06±0.04	0.01-0.14	0.10±0.04	0.01-0.16	0.07±0.05	0.01-0.18
H <sub>F</sub> <sup>+</sup> (M)	1.72±1.04	0.02-3.78	2.66±1.50	0.49-5.43	3.22±0.79	2.31-4.76	2.37±1.25	0.02-5.43
pH	(-0.20)±0.52	(-0.58)-1.81	(-0.31)±0.32	(-0.74)-0.31	(-0.50)±0.10	(-0.68)-(-0.36)	(-0.28)±0.42	(-0.74)-1.81
LWC (µg m <sup>-3</sup> )	66.64±46.51	2.68-184.71	42.88±28.80	6.60-86.03	51.65±17.69	30.51-101.12	57.2±37.15	2.68-184.71

787



788 Table 3: Regression analysis (Pearson's R) of PMF and TBM-resolved SOC<sub>s</sub>, SO<sub>2</sub>, NO<sub>2</sub>, ozone (O<sub>3</sub>), particle acidity (H<sub>p</sub><sup>+</sup>),  
 789 total particle-phase liquate water content (LWC<sub>P</sub>), and sulfate \*\*: P<0.01; \*: P<0.05. Note: R>0.5 are bold.

	Pearson's R								
	SOC_Iso	SOC_Mono	SOC_Cary	SOC_Nap	SOC_TBM	SOC_BB	SOC_SOA	SOC_SS	SOC_PMF
O <sub>3</sub> (ppb)	0.374**	.401**	0.011	0.246	.374**	-0.111	<b>.502**</b>	<b>.557**</b>	.434**
NO <sub>2</sub> (ppb)	.064	<b>.516**</b>	<b>.586**</b>	<b>.528**</b>	<b>.500**</b>	.469**	<b>.570**</b>	0.165	<b>.627**</b>
SO <sub>2</sub> (ppb)	0.044	0.198	.463**	.296*	0.255	.357*	0.035	-0.052	0.179
O <sub>x</sub> (μg m <sup>-3</sup> )	0.257	<b>.600**</b>	.433**	<b>.535**</b>	<b>.577**</b>	0.281	<b>.707**</b>	.445**	<b>.711**</b>
NO <sub>3</sub> (ppb)	.413**	<b>.530**</b>	0.101	.313*	.480**	-0.077	<b>.637**</b>	<b>.574**</b>	<b>.538**</b>
Sulfate (μg m <sup>-3</sup> )	.287*	<b>.610**</b>	.405**	<b>.506**</b>	<b>.579**</b>	0.23	<b>.646**</b>	<b>.886**</b>	<b>.799**</b>
H <sub>p</sub> <sup>+</sup> (M)	0.249	.334*	.391**	.388**	.395**	.400**	0.164	0.24	.376**
LWC <sub>P</sub> (μg m <sup>-3</sup> )	-0.18	0.18	0.115	0.209	0.113	0.003	.413**	.438**	.397**

790

791 Table 4: Results of multivariate linear analysis of PMF and TBM-resolved SOC<sub>s</sub>, O<sub>x</sub>, NO<sub>3</sub>, sulfate, particle acidity (H<sub>p</sub><sup>+</sup>), and  
 792 total particle-phase liquate water content (LWC<sub>P</sub>). \*\*: P<0.01; \*: P<0.05. Note: significant regressions are bold.

	normalized β-coefficient								
	SOC <sub>SS</sub>	SOC <sub>SOA</sub>	SOC <sub>BB</sub>	SOC <sub>PMF</sub>	SOC_Iso	SOC_Mono	SOC_Cary	SOC_Nap	SOC_TBM
O <sub>x</sub> (μg m <sup>-3</sup> )	<b>-0.453**</b>	0.355	<b>1.08**</b>	<b>0.59**</b>	-0.091	0.439*	<b>1.045**</b>	<b>0.739**</b>	0.537*
NO <sub>3</sub> (ppb)	<b>0.497**</b>	0.186	<b>-1.159**</b>	-0.289*	0.375	-0.066	<b>-0.999**</b>	-0.519*	-0.204
Sulfate (μg m <sup>-3</sup> )	<b>0.877**</b>	0.334*	0.164	<b>0.576**</b>	0.339	0.457*	0.323	0.258	0.439*
H <sub>p</sub> (M)	-0.141	-0.091	<b>0.386**</b>	0.087	-0.127	0.001	0.265	0.268	0.072
LWC <sub>P</sub> (μg m <sup>-3</sup> )	0.122	0.116	-0.166	0.029	-0.369	-0.14	-0.166	0.1	-0.194

793